Preparation, Structure, and Nuclear Magnetic Resonance Properties of the Nine-vertex *nido*-Rhenaborane $[(PMe_2Ph)_3H_2ReB_8H_{11}]$ * and Some Related Chemistry

Michael A. Beckett, Mark Bown, Xavier L. R. Fontaine, Norman N. Greenwood, John D. Kennedy, and Mark Thornton-Pett
School of Chemistry, University of Leeds, Leeds LS2 9JT

Thermolysis of [6,6,6-$(PMe_2Ph)_3$-6-H-*nido*-6-ReB_9H_{12}-9-(OEt)] (**1**) in $C_2D_2Cl_4$ solution gives the new, pale yellow air-stable compound [2,2,2-$(PMe_2Ph)_3$-2,2-H_2-*nido*-2-ReB_8H_{11}] (**2**) in 80% yield. Crystals of the CH_2Cl_2 hemisolvate of (**2**) are monoclinic, space group $P2_1/c$, with a = 1 130.0(3), b = 1 292.2(3), c = 2 424.0(5) pm, β = 94.15(2)°, and Z = 4; the molecular structure was refined to R = 0.0399, R' = 0.0454. The detailed n.m.r. behaviour of compound (**2**) together with data for previously reported rhodium and iridium analogues permits the location of the substituent site on previously unconfirmed [2-(CO)-2,2-$(PMe_3)_2$-*nido*-2-IrB_8H_{10}-3-Cl] and thence provides information on mechanistic pathways for the formation of these and related metallaboranes. Detailed n.m.r. data for the non-metalla analogues $[B_9H_{12}]^-$ and previously unassigned $[3\text{-}ClB_9H_{11}]^-$ provide information on their mechanism of formation and a comparison with the metallaborane analogues. The n.m.r. work includes extensive use of [^{11}B–^{11}B]-COSY and [^{1}H–^{1}H]-COSY experiments and establishes general points.

We have previously reported that the reaction of $[ReCl_3(PMe_2Ph)_3]$ with the *arachno*-$[B_9H_{14}]^-$ anion in ethanol solution results in the formation of a family of ten-vertex *nido*-6-rhenadecaboranes comprising $[(PMe_2Ph)_3HReB_9H_{13}]$, $[(PMe_2Ph)_3HReB_9H_{12}$-9-(OEt)], $[(PMe_2Ph)_3HReB_9H_{12}$-8-(OEt)], and $[(PMe_2Ph)_2ClHReB_9H_{12}$-2-$(PMe_2Ph)]$.[1] In the same paper we reported that the thermolysis, in *sym*-tetrachloroethane solution, of one of these products, the unsubstituted species $[(PMe_2Ph)_3HReB_9H_{13}]$, resulted in quantitative chlorination to give the 2-chloro-*nido*-6-rhenadecaborane $[(PMe_2Ph)_3HReB_9H_{12}$-2-Cl], in which the integrity of the *nido* ten-vertex cluster was retained. We have now found, by contrast, that an analogous treatment of the 9-ethoxy-substituted *nido*-6-rhenadecaborane $[(PMe_2Ph)_3HReB_9H_{12}$-9-(OEt)] results instead in a quantitative cluster degradation, to give the nine-vertex *nido*-rhenanonaborane $[(PMe_2Ph)_3H_2ReB_8H_{11}]$, for which we here also report the molecular structure and some details of the multielement n.m.r. chemical shift and coupling constant behaviour. These n.m.r. data, together with those for the non-metal-containing *nido* nine-vertex anions $[B_9H_{12}]^-$ and $[3\text{-}ClB_9H_{11}]^-$, and those for the other known *nido* nine-vertex metallanonaboranes $[(CO)(PMe_3)_2IrB_8H_{11}]$,[2,3] $[(CO)(PMe_3)_2IrB_8H_{10}$-3-Cl],[3] and $[(C_5Me_5)RhB_8H_{10}(PMe_2Ph)]$,[4] reveal diagnostically useful n.m.r. behavioural patterns, and also thereby throw light on the gross mechanistic pathways involved in the cluster closure and degradation processes that yield these various *nido* nine-vertex species. The cluster numbering schemes used for the *nido* ten-vertex, *arachno* nine-vertex, and *nido* nine-vertex clusters are given in structures (**I**)—(**III**). Ten-vertex ⟶ nine-vertex cluster conversion and *arachno* ⟷ *nido* nine-vertex cluster interconversions change the numbering associated with particular boron atoms, but reference to structures (**I**)—(**III**) should minimise confusion.

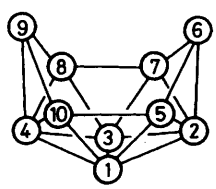

(**I**)

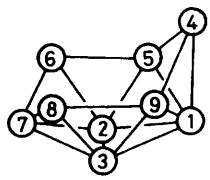

(**II**)

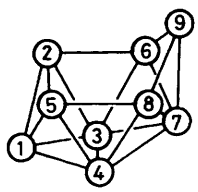

(**III**)

Results and Discussion

(*a*) *Preparation of the Nine-vertex* nido-*Rhenaborane.*—Heating of a sample of the *nido* ten-vertex species [6,6,6-$(PMe_2Ph)_3$-6-H-*nido*-6-ReB_9H_{12}-9-(OEt)][1] (**1**) in *sym*-$C_2D_2Cl_4$ solution [equation (1)] results in a near-quantitative yield of the new nine-vertex *nido* cluster compound [2,2,2-$(PMe_2Ph)_3$-2,2-H_2-*nido*-2-ReB_8H_{11}] (**2**). The new rhenanonaborane was identified by *X*-ray crystallography and n.m.r. spectroscopy as described below. Isolation of the pure product was readily effected by preparative thin-layer chromatography in air, yields of *ca.* 80% of the very pale yellow pure crystalline compound being obtained from reactions conducted on the 0.1-mmol scale. Monitoring the reaction by ^{31}P n.m.r. spectroscopy showed that it is complete in *ca.* 45 min at 373 K, with the integrated spectra showing that the incidence of phosphorus-containing by-products was ≤*ca.* 5%.

* 2,2,2-Tris(dimethylphenylphosphine)-2,2-dihydrido-2-rhena-*nido*-nonaborane.

Supplementary data available: see Instructions for Authors, *J. Chem. Soc., Dalton Trans.*, 1988, Issue I, pp. xvii—xx.

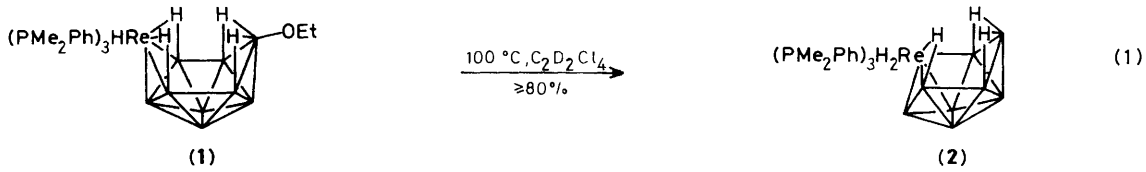

(1)

The new nine-vertex *nido* rhenaborane compound (**2**) is air-stable for weeks in crystalline form, as are its iridaborane and rhodaborane analogues $[(CO)(PMe_3)_2IrB_8H_{11}]$[2,3] and $[(C_5Me_5)RhB_8H_{10}(PMe_2Ph)]$.[4] In contrast to the behaviour of $[(CO)(PMe_3)_2IrB_8H_{10}Cl]$,[2] however, we have not been able to induce further condensation to give a closed deltahedral species. Instead, further heating of compound (**2**) in a variety of solvents resulted in a general decomposition with no viable yields of any other rhenaborane species on the scale that the reactions were investigated [10—100 μmol of (**2**)].

The initial near-quantitative degradation of the ten-vertex rhenaethoxydecaborane precursor (**1**) is of interest because it involves the clean elimination of one boron vertex from the cluster. As mentioned in the Introduction, the quantitative chlorinating ability of $C_2D_2Cl_4$ is already recognised in *nido*-6-rhenadecaborane chemistry,[1] and this therefore suggests straightforward stoicheiometries such as that in equation (2) to

$$\underset{(1)}{[(PMe_2Ph)_3HReB_9H_{12}(OEt)]} + C_2D_2Cl_4 \longrightarrow \underset{(2)}{[(PMe_2Ph)_3H_2ReB_8H_{11}]} + \{B(OEt)Cl_2\} + \{CDCl{=}CDCl\} \quad (2)$$

account for the products, particularly in view of the somewhat greater stability of compound (**2**) in solvents such as $CD_3C_6D_5$.

However, no major peaks in the ^{11}B n.m.r. spectrum of the product mixture had chemical shifts corresponding to three-co-ordinate electronegatively substituted boron[5,6] [although there were two strong singlet peaks in the four-co-ordinate region[5,6] at $\delta(^{11}B)$ +5.3 and +0.4 p.p.m.], and so the overall stoicheiometry of the process is probably more complex than this. It can be noted parenthetically that the reaction involves removal of the elements of B(OEt) and the retention of the 13 H atoms and three phosphine ligands on the cluster.

(*b*) *Molecular Structure.*—Crystals (of the CH_2Cl_2 hemisolvate) suitable for single-crystal *X*-ray diffraction analysis were obtained from dichloromethane–diethyl ether. An ORTEP drawing of the molecular structure obtained by this diffraction analysis is given in Figure 1, with selected P-organyl group atoms omitted for clarity. Selected interatomic distances and angles are given in Tables 1 and 2 respectively, and fractional atomic co-ordinates are given in Table 8 in the Experimental section. All hydrogen atoms were located, except those bound directly to the rhenium atom: n.m.r. spectroscopy [see section (*c*) below] shows that there are three of these. One is a bridging hydrogen atom at Re(2)–H–B(5). This is in a position analogous to that of H(2,5) in the *nido*-anion $[B_9H_{12}]^-$,[7] and is

Table 1. Selected interatomic distances (pm) for $[2,2,2\text{-}(PMe_2Ph)_3\text{-}2,2\text{-}H_2\text{-}nido\text{-}2\text{-}ReB_8H_{11}]$, with estimated standard deviations (e.s.d.s) in parentheses

(*i*) From the rhenium atom			
Re(2)–P(1)	242.9(4)	Re(2)–B(1)	220.7(12)
Re(2)–P(2)	243.2(5)	Re(2)–B(3)	238.7(13)
Re(2)–P(3)	243.1(4)	Re(2)–B(5)	252.7(13)
		Re(2)–B(6)	248.3(13)
(*ii*) Boron–boron			
B(1)–B(3)	175.0(19)	B(4)–B(8)	174.7(18)
B(1)–B(4)	172.7(18)	B(5)–B(8)	187.4(19)
B(1)–B(5)	176.4(17)	B(6)–B(7)	178.5(17)
B(3)–B(4)	180.8(19)	B(6)–B(9)	180.4(17)
B(3)–B(6)	180.3(17)	B(7)–B(8)	178.2(18)
B(3)–B(7)	184.5(18)	B(7)–B(9)	166.8(17)
B(4)–B(5)	173.3(19)	B(8)–B(9)	180.7(19)
B(4)–B(7)	178.2(21)		
(*iii*) Boron–hydrogen			
B(1)–H(1)	120(4)	B(6)–H(6,9)	132(4)
B(3)–H(3)	114(4)	B(9)–H(6,9)	119(6)
B(4)–H(4)	141(5)	B(9)–H(8,9)	130(4)
B(5)–H(5)	113(4)	B(8)–H(8,9)	118(5)
B(6)–H(6)	124(4)		
B(7)–H(7)	106(5)		
B(8)–H(8)	109(5)		
(*iv*) Other			
P(1)–C	181.0(12)—183.3(13)	P(3)–C	181.5(11)—184.8(7)
P(2)–C	182.4(12)—183.6(8)		

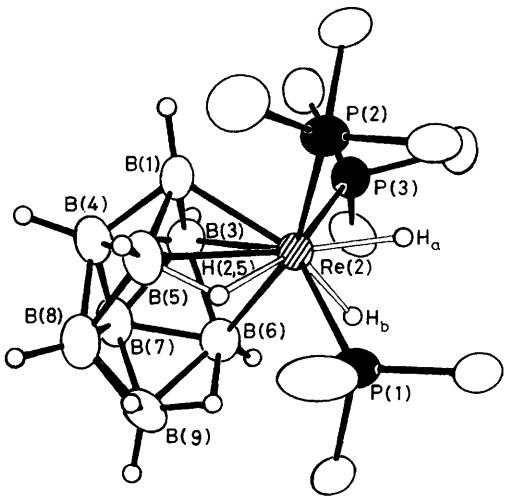

Figure 1. ORTEP drawing of the crystallographically determined molecular structure of $[(PMe_2Ph)_3H_2ReB_8H_{11}]$ (**2**), with organyl hydrogen and aromatic carbon atoms (apart from the *ipso* ones) omitted. The two Re–H terminal and one Re–H–B(5) bridging hydrogen atoms were apparent from n.m.r. experiments. They were not located in the diffraction analysis but were positioned by potential-minima calculations.[8,9] In these calculations the Re–H(terminal) distances were set at 168 pm [see R. G. Teller and R. Bau, *Struct. Bonding* (*Berlin*), 1981, **44**, 62] and the H(2,5) bridging atom position was the minimum located by setting the B–H and Re–H distances to corresponding distances observed in the previously determined structure $[(PMe_2Ph)_3HReB_9H_{12}(PMe_2Ph)]$.[1] The three hydrogen atoms located were subsequently co-refined to allow for interhydrogen interactions, fractional co-ordinates ($\times 10^4$, *cf.* Table 8) for the H(2,5) atom then being 1 150, 3 204, 2 020 and for the two Re–H(5) atoms being 3 231, 3 212, 1 366 and 2 053, 2 509, 0 904

Table 2. Selected angles (°) between interatomic vectors for $[(PMe_2Ph)_3H_2ReB_8H_{11}]$, with e.s.d.s in parentheses

(*i*) At the rhenium atom							
P(1)–Re(2)–P(2)	93.5(2)					B(1)–Re(2)–B(3)	44.6(4)
P(1)–Re(2)–P(3)	132.5(1)	P(2)–Re(2)–P(3)	94.5(2)			B(1)–Re(2)–B(5)	43.1(4)
P(1)–Re(2)–B(1)	136.5(3)	P(2)–Re(2)–B(1)	78.2(4)	P(3)–Re(2)–B(1)	90.9(4)	B(1)–Re(2)–B(6)	83.2(5)
P(1)–Re(2)–B(3)	135.6(3)	P(2)–Re(2)–B(3)	120.9(4)	P(3)–Re(2)–B(3)	76.0(4)	B(3)–Re(2)–B(5)	64.7(5)
P(1)–Re(2)–B(5)	94.1(4)	P(2)–Re(2)–B(5)	85.1(4)	P(3)–Re(2)–B(5)	133.2(3)	B(3)–Re(2)–B(6)	43.4(4)
P(1)–Re(2)–B(6)	95.8(5)	P(2)–Re(2)–B(6)	160.4(3)	P(3)–Re(2)–B(6)	92.0(4)	B(5)–Re(2)–B(6)	77.0(5)
(*ii*) Rhenium boron boron							
Re(2)–B(1)–B(3)	73.2(6)	Re(2)–B(3)–B(1)	62.3(6)	Re(2)–B(5)–B(1)	58.7(5)	Re(2)–B(6)–B(3)	65.5(6)
Re(2)–B(1)–B(4)	111.3(8)	Re(2)–B(3)–B(4)	101.0(7)	Re(2)–B(5)–B(4)	98.0(7)	Re(2)–B(6)–B(7)	112.1(7)
Re(2)–B(1)–B(5)	78.2(6)	Re(2)–B(3)–B(6)	71.1(6)	Re(2)–B(5)–B(8)	111.5(7)	Re(2)–B(6)–B(9)	116.4(7)
		Re(2)–B(3)–B(7)	114.0(7)				
(*iii*) Other							
B(1)–B(3)–B(6)	122.8(6)	B(3)–B(6)–B(9)	111.6(9)	Re(2)–P(1)–C	115.9(5)—117.1(4)	B–B–H(*exo*)	102.0(19)—137.7(18)
B(1)–B(5)–B(8)	113.1(9)	B(5)–B(8)–B(9)	114.9(9)	Re(2)–P(2)–C	116.8(3)—120.0(5)	Re(2)–B–H(*exo*)	118.7(30)—130.9(31)
B(3)–B(1)–B(5)	97.0(8)	B(6)–B(9)–B(8)	100.0(8)	Re(2)–P(3)–C	113.4(4)—120.6(4)		

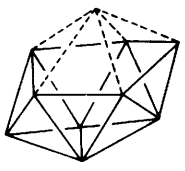

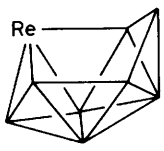

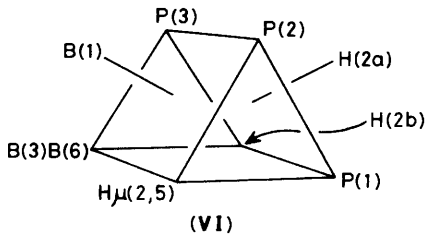

therefore approximately *trans* to P(3). The other two are in mutually inequivalent Re-terminal positions, and preliminary[8] results of potential-well calculations using modified Orpen HYDEX programs[9] indicate that these are at the positions indicated.

The structure of the nine-atom ReB_8 cluster is seen to be based on that of the ten-vertex *closo* bicapped square antiprism [structure (**IV**)], with one tropical (five-connected) vertex missing, and the metal atom occupying a position on the open face on the second four-atom tropical belt [structure (**V**)]. The cluster structure is thus analogous to those established crystallographically for the *nido* nine-vertex species $[(CO)(PMe_3)_2IrB_8H_{11}]$[3] and for the *nido* anion $[B_9H_{12}]^-$ itself.[7]

Within the ReB_8 cluster, the Re(2)–B(3) distance of *ca.* 239 pm is just within the range of 232—239 pm previously established in (two) ten-vertex *nido*-6-rhenadecaboranes,[1] but the Re(2)–B(1) distance is substantially shorter at *ca.* 221 pm, this behaviour being paralleled by the corresponding short B(1)–B(2) and B(1)–Ir(2) distances in $[B_9H_{12}]^-$ and $[(CO)(PMe_3)_2IrB_8H_{11}]$ respectively,[3,7] and also by the corresponding B(1)–B(2)-type distances in *closo*-$[B_{10}H_{10}]^{2-}$.[10] The interboron distances involving B(1) in compound (**2**) are also somewhat shorter than average, perhaps therefore indicating the incidence of some *closo*-$[B_{10}H_{10}]^{2-}$ character within this square-pyramidal unit [see also section (*d*) below]. Conversely, the rhenium–boron distances Re(2)–B(5) (H-bridged) and Re(2)–B(6) (unbridged) in the open face are long at *ca.* 253 and 248 pm respectively, but again this behaviour is paralleled by the corresponding long Ir–B and B–B distances in $[(CO)(PMe_3)_2IrB_8H_{11}]$ and $[B_9H_{12}]^-$ [and also by B(5)–B(8) in the rhenaborane], indicating that this is also a general characteristic of the *nido* nine-vertex cluster type.

As with the neutral iridium centre $Ir(CO)(PMe_3)_2$ in the iridaborane analogue $[(CO)(PMe_3)_2IrB_8H_{11}]$,[3] the neutral metal centre $ReH_2(PMe_2Ph)_3$ in the rhenaborane described here may be regarded as a straightforward three-orbital three-electron contributor to the cluster bonding scheme, equivalent to a binary borane BH^- unit. The metal centre therefore formally has an eighteen-electron d^2 rhenium(V) configuration, with eight valence orbitals involved in bonding. This configuration is similar to that of the d^2 tungsten(IV) centre in the recently reported ten-vertex *nido*-6-wolfradecaborane $[(PMe_2Ph)_3H_2WB_9H_{13}]$,[11] and, in accord with this parallel, the *exo*-polyhedral metal ligation of the nine-vertex rhenaborane also exhibits fluxional behaviour, as discussed in the n.m.r. section (*c*) below. In this *exo*-polyhedral metal–ligand sphere the rhenium–phosphorus distances are at the upper end of the range of 235.6—243.6 pm previously established for the formal rhenium(III) centres in the ten-vertex *nido*-6-rhenadecaboranes,[1] and are more nearly comparable with the tungsten–phosphorus distances of 242.2—249.4 pm found for the compound $[(PMe_2Ph)_3H_2WB_9H_{13}]$.[11] The eight two-electron bonding vectors appear to be directed approximately towards the corners of a bicapped (square face) trigonal prism [structure (**VI**)], one of the three cluster-bonding vectors being transoid to P(3) and directed towards the Re(2)B(5) bridging hydrogen atom, the other two presumably being directed principally towards B(1) and B(3)B(6) as discussed previously for the iridium analogue $[(CO)(PMe_3)_2IrB_8H_{11}]$.[3]

(*c*) *Nuclear Magnetic Resonance Properties of the* nido-*Rhenanonaborane and Other Related Species.*—The ^{11}B and ^1H n.m.r. parameters for the metallaborane cluster of $[(PMe_2Ph)_3H_2ReB_8H_{11}]$ (**2**) are given in Table 3, together with those of the analogous metallaboranes $[(CO)(PMe_3)_2IrB_8H_{11}]$,[3] $[(CO)(PMe_3)_2IrB_8H_{10}Cl]$,[3] and $[(C_5Me_5)RhB_8H_{10}(PMe_2Ph)]$[4] for comparison. The 128-MHz ^{11}B and ^{11}B-{^1H(broad-band noise)} spectra of compound (**2**) are illustrated in Figure 4 below. Figure 4 also shows a 'two-dimensional' [^{11}B–^{11}B]-COSY plot, also recorded with {^1H(broad-band noise)}

Table 3. Boron-11 and proton n.m.r. data for the metallaborane clusters $[(PMe_2Ph)_3H_2ReB_8H_{11}]$,[a] $[(CO)(PMe_3)_2IrB_8H_{11}]$,[b] $[(CO)(PMe_3)_2IrB_8H_{10}Cl]$,[b] and $[(C_5Me_5)RhB_8H_{10}(PMe_2Ph)]$[c]

	$[(PMe_2Ph)_3H_2ReB_8H_{11}]$[a] CD_2Cl_2 solution at 294 K		$[(CO)(PMe_3)_2IrB_8H_{11}]$[b] $CDCl_3$ solution at 294 K		$[(CO)(PMe_3)_2IrB_8H_{10}Cl]$[b] $CDCl_3$ solution at 294 K		$[(C_5Me_5)RhB_8H_{10}(PMe_2Ph)]$[c] $CDCl_3$ solution at 294 K	
Assignment[d]	$\delta(^{11}B)$[e,f]	$\delta(^1H)$[g,h]	$\delta(^{11}B)$[e]	$\delta(^1H)$[g]	$\delta(^{11}B)$[e]	$\delta(^1H)$[g]	$\delta(^{11}B)$[e]	$\delta(^1H)$[g]
1	+28.9	+5.26	+23.1	+5.04	+22.1	+5.06	+39.4	+5.82
4	+7.9	+4.14	+8.8	+4.90	+13.5	+5.32	+5.3	+2.55, +3.26
6	−5.0	+2.73	−5.3	+2.94	−3.5	+3.05	+3.9	
9	*ca.* −16.0[i]	+2.42	−14.5	+2.99	−14.0	+3.05	−16.6	+2.78
8	*ca.* −16.0[i]	+0.83	−13.6	+1.02	−9.0	+1.50	−12.3	+1.50
3	−18.3	+0.17	−15.3	+0.83	+1.1[j]	*j*	−10.7	+0.95
5	−46.3	−0.30	−39.9	−0.51	−40.8	−0.87	−42.8[k]	*k*
7	−53.2	−1.39	−52.5	−1.48	−47.4	−1.19	−46.2	−0.95
μ(6,9)(bridge)	—	−3.81	—	−2.10	—	−2.03	—	−0.37
μ(8,9)(bridge)	—	−3.89	—	−2.96	—	−2.50	—	−2.63
μ(2,5)(bridge)	—	−14.09[l,m]	—	−14.50[l,n]	—	−14.60[l,o]	—	−13.60[l,p]
2(*i.e.* M–H)	—	−4.78,[q] −9.12[r]	—	—	—	—	—	—

[a] This work. [b] Data from ref. 3. [c] Data from ref. 4. [d] Numbering as in Figure 1 and structure (**III**); assignments by ^1H-$\{^{11}B\}$ spectroscopy (compare ref. 3) together with two-dimensional COSY ^1H–^1H and ^{11}B–^{11}B spectroscopy (Table 4). [e] $\delta(^{11}B)$ in p.p.m., ±0.5 p.p.m. to high frequency (low field) of $BF_3(OEt_2)$ in $CDCl_3$ solution (ref. 6). [f] Note small changes in $\delta(^{11}B)$ with solution conditions (*e.g.* Table 4). [g] $\delta(^1H)$ ±0.05 p.p.m. to high frequency (low field) of internal $SiMe_4$. [h] Proton resonances assigned to directly bound boron positions by selective ^1H-$\{^{11}B\}$ spectroscopy. [i] Accidentally coincident resonances. [j] Site of chlorine substituent. [k] Site of phosphine substituent, $^1J(^{31}P$–$^{11}B) = 125$ Hz (ref. 4). [l] Selectively sharpened by $\nu[^{11}B(5)]$ in ^1H-$\{^{11}B$(selective)$\}$ experiments. [m] Doublet, $^2J(^{31}P$–Re–$^1H)$ 32 Hz plus additional fine structure implying two $^2J(^{31}P$–Re–$^1H)$ of ≤ *ca.* 5 Hz. [n] $^2J(^{31}P$–Ir–$^1H)$ 62 Hz. [o] $^2J(^{31}P$–Ir–$^1H)$ 49 Hz. [p] $^2J(^{31}P$–B–$^1H)$ 25 Hz. [q] At 278 K; doublet [$^2J(^{31}P$–Re–$^1H)$ 51 Hz] of triplets [two $^2J(^{31}P$–Re–$^1H)$ of *ca.* 29 Hz]. [r] At 278 K; triplet [two $^2J(^{31}P$–Re–$^1H)$ *ca.* 32 Hz and one $^2J(^{31}P$–Re–$^1H)$ *ca.* zero].

Table 4. Interboron and interproton two-dimensional COSY correlations for the metallaborane cluster $[(PMe_2Ph)_3H_2ReB_8H_{11}]$

	^{11}B; $CD_3C_6D_5$ solution at 353 K			^1H; CD_2Cl_2 solution at 294 K	
Assignment[a]	$\delta(^{11}B)$/p.p.m.[b]	$[^{11}B$–$^{11}B]$-COSY correlations[c,d]	$^1J(^{11}B$–$^1H)$/Hz	$\delta(^1H)$/p.p.m.	$[^1H$–$^1H]$-COSY correlations[c,e]
(1)	+30.2	(3)s, (4)w, (5)m	151	+5.26	(3)w, (4) m (see footnote *e*)
(2)	(Re atom)	—	—	−4.78,[f] −9.12[f]	—
(3)	−17.9	(1)s, (4)m, (6)s, (7)m, (8)w?	134	+0.17	(1)w, (4)m, (5)w?$_4$, (6)m, (7)w, (8)w?$_4$, μ(6,9)s
(4)	+10.0	(1)w, (3)m, (5)w, (7)s, (8)m	141	+4.14	(1)m, (3)m, (7)w, (8)s, μ(8,9)m, μ(2,5)s
(5)	−44.7	(1)m, (4)w, (8)w	147	−0.30	(3)w?$_4$, (8)w, μ(2,5)s (see footnote *e*)
(6)	−3.8	(3)s, (7)m	159	+2.73	(3)m, (7)w, (8)m$_4$, μ(6,9)s$_2$, μ(8,9)w
(7)	−52.0	(3)m, (4)s, (6)m, (8)s, (9)s	147	−1.39	(3)w, (4)w, (6)m, (9)s (see footnote *e*)
(8)	−15.0	(3)w?, (4)m, (5)w, (7)s	*ca.* 150	+0.83	(3)w?$_4$, (4)s, (5)w, (6)m$_4$, μ(6,9)w, μ(8,9)s$_2$, μ(2,5)w
(9)	−15.5	(7)s	*ca.* 150	+2.42	(7)s, μ(6,9)s$_2$, μ(8,9)s$_2$, μ(2,5)w
μ(6,9)	—	—	< 50	−3.81	(3)s, (6)s$_2$, (8)w, (9)s$_2$
μ(8,9)	—	—	< 50	−3.89	(4)s, (6)m, (8)s$_2$, (9)s$_2$
μ(2,5)	—	—	< 50	−14.09	(4)s, (5)s$_2$, (8)w, (9)w$_4$

[a] Numbering as in Figure 1 and structure (**III**). [b] $\delta(^{11}B)$ ±0.5 p.p.m. to high frequency (low field) of Ξ 32 031 971 Hz [nominally $BF_3(OEt_2)$ in $CDCl_3$ solution; ref. 6]. Note small differences in $\delta(^{11}B)$ with solution conditions (compare Table 3). [c] Observed correlations under the conditions stated are designated stronger (s), weaker (w), or intermediate (m). [d] The strength of the correlation will depend upon solution conditions as well upon interboron coupling constants (see ref. 6). [e] Obtained under ^1H-$\{^{11}B$(broad-band noise)$\}$ conditions; some ^1H–^1H correlations for H(1), H(5), and H(7) may be weaker or not observed because of the difficulty of achieving complete $\{^{11}B\}$ decoupling over the entire $\nu(^{11}B)$ range of *ca.* 10 kHz (*i.e.* 80 p.p.m. at 128 MHz). Numerical subscripts refer to *n* in $^nJ(^1H$–$^1H)$ when $n \neq 3$; note that in polyhedral chemistry *n* does not necessarily imply *n* two-electron three-centre bonds (see refs. 6 and 33). [f] These $\delta(^1H)$ values for 278 K; no correlations observed at 294 K, perhaps due to incipient rapid exchange (see text and Table 5).

decoupling, and recorded at elevated temperatures in order to minimise ^{11}B-relaxation broadening[6] and thus enhance any observable off-diagonal correlations. The observed two-dimensional $[^{11}B$-$^{11}B]$-COSY correlations are summarised in Table 4, along with two-dimensional $[^1H$-$^1H]$-COSY[12,13] correlations recorded under conditions of $\{^{11}B$(broad-band noise)$\}$ decoupling. A picture of the ^1H–^1H correlation plot, together with a one-dimensional ^1H-$\{^{11}B$(broad-band noise)$\}$ spectrum, is given in Figure 5 below. N.m.r. parameters for the rhenium-bound phosphine ligands and hydrogen atoms are given in Table 5.

For the rhenaborane (**2**), the marked similarity of the cluster ^{11}B and ^1H shielding behaviour to that of the iridaborane analogue $[(CO)(PMe_3)_2IrB_8H_{11}]$ reported previously[3] (Table 3 and Figures 2 and 3) clearly confirms the similarity of electronic constitution evident from the structural similarities discussed in the previous section (*b*). Also as with the iridaborane reported previously,[3] the behaviour of the bridging proton resonances in ^1H-$\{^{11}B$(selective)$\}$ experiments permits the tentative assignment of particular ^{11}B resonances in the open-face positions. The results of two-dimensional $[^{11}B$-$^{11}B]$-COSY[6,14–16] experiments on compound (**2**) (Table 4), and also on the rhodaborane analogue $[(C_5Me_5)RhB_8H_{10}(PMe_2Ph)]$ as discussed elsewhere,[4] then permit the confirmation of these

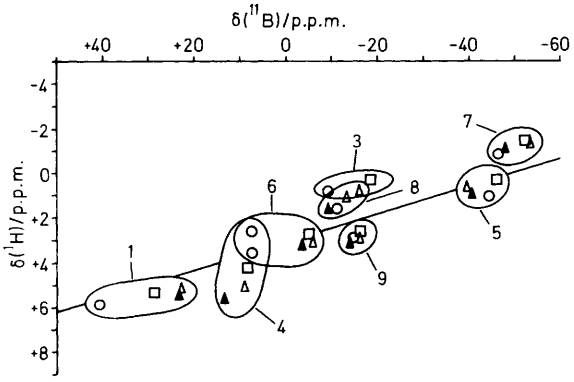

Figure 2. Proton boron-11 shielding correlation plot [$\delta(^1H)$ *versus* $\delta(^{11}B)$] for the *nido*-2-metallanonaboranes $[(PMe_2Ph)_3H_2ReB_8H_{11}]$ (□), $[(C_5Me_5)RhB_8H_{10}$-5-$(PMe_2Ph)]$ (○), $[(CO)(PMe_3)_2IrB_8H_{11}]$ (△), and $[(CO)(PMe_3)_2IrB_8H_{10}$-3-Cl] (▲). The labelled cartouches summarise the positional assignments [numbering as in structure (**III**) and Figure 1; see Table 3], and the line drawn has a slope corresponding to a $\delta(^1H):\delta(^{11}B)$ ratio of 1:13, with intercept $\delta(^1H) = +3.0$ p.p.m.

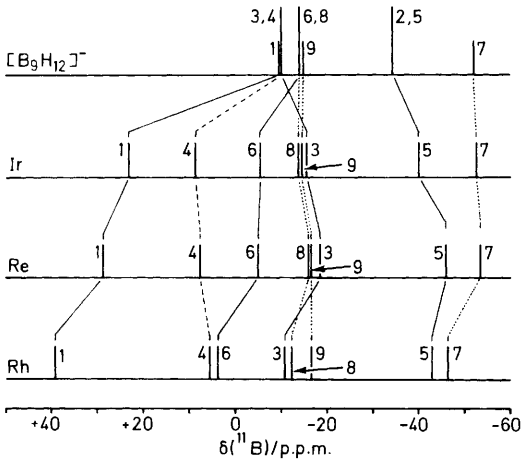

Figure 3. Stick diagram of the ^{11}B n.m.r. positions for $[(C_5Me_5)RhB_8H_{10}(PMe_2Ph)]$ (representation Rh), $[(PMe_2Ph)_3H_2ReB_8H_{11}]$ (representation Re), $[(CO)(PMe_3)_2IrB_8H_{11}]$ (representation Ir), and the binary borane anion $[B_9H_{12}]^-$ (compare Figure 4 in ref. 11). In the metallaboranes it can be seen that the basic shielding pattern of the $[B_9H_{12}]^-$ B(3)B(4)B(8)B(9)B(6)B(7) pentagonal-pyramidal fragment is retained, but that the metal induces large shielding changes in its nearest-neighbour boron atoms [compare ref. 59 for other shielding changes observed in subrogated *nido* nine-vertex borane derivatives; (——) adjacent (α) to the metal atom, (...) meta (β) to the metal atom, and ( ) antipodal (in this case also β) to the metal atom; note that the numbering scheme used in refs. 7 and 59 differs from that which we use here]

assignments together with the assignment of the remainder of the ^{11}B spectrum (Table 3), and thence by analogy (Figures 2 and 3) also permit the assignment of the unsubstituted iridium analogue $[(CO)(PMe_3)_2IrB_8H_{11}]$. Selective ^1H-$\{^{11}B\}$ spectroscopy assigns the ^1H resonances to their directly bound boron positions, and the results of two-dimensional [^1H-^1H]-COSY[12,13] experiments (Table 4 and Figure 5 below) then enable the confirmation of the positional assignments and also permit the assessment of the incidence and relative magnitude of ^1H-^1H correlations in this cluster type. This new application of the [^1H-^1H]-COSY technique has great potential as a structural tool in polyhedral boron chemistry,[12,13] but so far it has been applied only to a limited[13,17–24] extent in the general case [see also section (*d*) below, near Table 6].

In the positional assignments of Table 3, the only two ambiguities then remaining are (*a*) the assignments for both ^{11}B and ^1H between the 3 and 8 positions in the iridaborane $[(CO)(PMe_3)_2IrB_8H_{11}]$ (though this is not critical for assessing shielding patterns because the resonance positions are so close), and (*b*) the assignment of the resonances at $\delta(^1H)$ +2.55 and +3.26 p.p.m. between H(4) and H(6) in the rhodaborane $[(C_5Me_5)RhB_8H_{10}(PMe_2Ph)]$. Of these last two, we would tentatively assign the lower-field resonance at $\delta(^1H)$ +3.26 p.p.m. to H(4), and that at +2.55 p.p.m. to H(6) by analogy with the other compounds (Figure 2), although the magnetic anisotropy of the neighbouring C_5Me_5 or PMe_2Ph groups may affect the ^1H shielding at these particular positions. Again, however, the resonance positions are so close that the distinction is not critical for assessing patterns in shielding behaviour.

The utility of these detailed assignments is illustrated in Figure 2, which presents a plot of $\delta(^1H)$ *versus* $\delta(^{11}B)$ for directly bound B–H in $[(PMe_2Ph)_3H_2ReB_8H_{11}]$, $[(C_5Me_5)RhB_8H_{10}(PMe_2Ph)]$,[4] $[(CO)(PMe_3)_2IrB_8H_{11}]$,[3] and in the chlorinated iridaborane $[(CO)(PMe_3)_2IrB_8H_{10}Cl]$.[3] It should be noted that the ^1H data are those measured in the essentially diluent solvents CD_2Cl_2 and $CDCl_3$; use of anisotropic, Lewis-acidic, or donor solvents can produce local effects[6,25,26] which could confuse detailed comparisons. It is apparent from Figure 2 that the ^{11}B–^1H data for particular positional sites are closely grouped. This type of grouping phenomenon is also a potentially useful structural tool that has not yet been applied in the general case. In the present case, as mentioned above, it now permits the reasonable, complete assignment of the ^1H and ^{11}B spectra of $[(CO)(PMe_3)_2IrB_8H_{11}]$, and also confirms that the chlorine substituent is at the 3-position in $[(CO)(PMe_3)_2IrB_8H_{10}Cl]$ because this compound does not have a ^{11}B–^1H datum in the region of the cartouche for the 3-position in Figure 2 [the 8-position, which occurs in a similar region of the plot, is discounted on the basis that selective ^1H-$\{^{11}B(3)\}$ experiments[3] on $[(CO)(PMe_3)_2IrB_8H_{10}Cl]$ produce no selective sharpening of the $^1H(8,9)$-(bridge) resonance]. This confirmation of 3-substitution is useful in assessing mechanistic pathways [see section (*d*) below, near Scheme].

A second use of these assignments is that they now permit a comparison of the ^{11}B shielding patterns in the nine-vertex *nido*-2-metallanonaboranes with those of the 'parent' binary borane model $[B_9H_{12}]^-$. This was not previously possible because the spectrum of the $[B_9H_{12}]^-$ anion had also not been previously assigned [see now section (*d*) below, near Table 6] and at first sight the shielding patterns for the metallaboranes and the $[B_9H_{12}]^-$ anion appear to be considerably different.[3] A stick diagram of the ^{11}B n.m.r. spectra of the metallaboranes and of $[B_9H_{12}]^-$ is given in Figure 3. The similarity of the shielding patterns among the three metallaboranes represented is again apparent (the deviation for the chloro-substituted iridaborane, not represented in Figure 3, has been discussed elsewhere),[3] and the diagram also shows that the principal differences in the gross shielding patterns between these and $[B_9H_{12}]^-$ arise from the differences at B(1), B(4), and B(6). Of these, the apical B(1) and open-face B(6) positions, which exhibit deshieldings in the ranges of 32—48 and 9—17 p.p.m. respectively, are adjacent to the metal atom but the B(4) position, with deshieldings of 16—18 p.p.m., is in a quasi-antipodal position with respect to the metal across the base of the square-pyramidal B(1)M(2)B(3)-B(4)B(5) cap (compare shielding effects in five-vertex *nido*-2-metallaborane clusters[27–29]). This, together with the increases

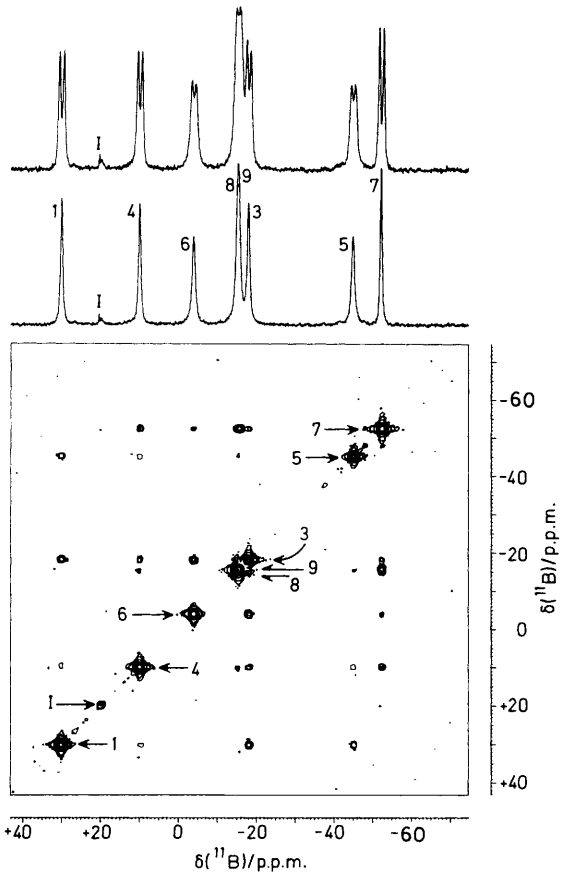

Figure 4. 128-MHz ^{11}B N.m.r. spectra for $[(PMe_2Ph)_3H_2ReB_8H_{11}]$ (**2**): the top trace is the ^{11}B spectrum, the centre trace is the ^{11}B-$\{^1H$(broad-band noise)$\}$ spectrum, and the lowest diagram is a (symmetrized) homonuclear two-dimensional COSY-90 plot using data acquired under conditions of $\{^1H$(broad-band noise)$\}$ decoupling. The experiments were performed on a solution of (**2**) in $CD_3C_6D_5$ at elevated temperatures to minimise relaxation problems; I = principal impurity peaks

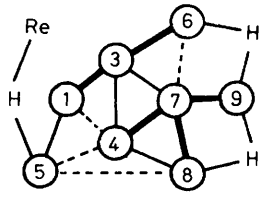

(VII)
Observed $^{11}B-^{11}B$ COSY correlations in compound (**2**)

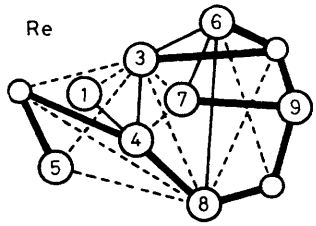

(VIII)
Observed $^1H-^1H$ COSY correlations in compound (**2**)

of shielding of some 6—11 p.p.m. at the B(5) position adjacent to the metal, suggests that the replacement of B(2) by a metal centre has caused significant modification of the electronic structure of this square-pyramidal cap, although geometrical similarities suggest that low metal-centred excitation energies may also be significant in this regard.[30] Such a modification is however perhaps not surprising, but it is also thereby clear that the influence of the iridium and rhenium centres is different from the effect of similar centres when in the 6-position of a ten-vertex *nido*-decaboranyl cluster, where they produce only minor perturbations in the basic shielding pattern of the parent $B_{10}H_{14}$.[11] On the other hand, however, it should be pointed out that moieties such as 6-$Ru(C_6Me_6)$, 6-$Os(C_6Me_6)$, and 6-$Rh(C_5Me_5)$ in the *nido*-decaboranyl cluster *do* induce marked nuclear deshieldings of some 20—25 p.p.m. on their adjacent B(2) and B(5)(7) atoms [*nido* ten-vertex numbering system, structure (**I**)],[16,30] which underscores the continued need for comprehensive and systematic assignment work for the establishment of diagnostically useful general shielding rules in these and related areas.

The two-dimensional $[^{11}B-^{11}B]$-COSY,[6,14,15] and, more particularly, the two-dimensional $[^1H-^1H]$-COSY [12,13] n.m.r. techniques, as applied to polyhedral boron-containing compounds, are still novel, and certain aspects arising from this work merit comment. The three organophosphine ligands on the rhenaborane (**2**) mean that this is quite a bulky molecule (82 atoms). There will therefore be significant relaxation broadening of the ^{11}B resonances at lower temperatures in solution, and the $[^{11}B-^{11}B]$-COSY experiments were therefore carried out at higher temperatures (in perdeuteriotoluene solution) to clarify the stronger correlations and to render the weaker ones more observable. Under these conditions (Figure 4 and Table 4) interboron correlations were apparent between all adjacent pairs of boron atoms except for the hydrogen-bridged (6)(9) and (8)(9) pairs. There is, however, precedent for the absence of observable correlations for hydrogen-bridged sites,[6,14-16] and this absence does not in fact inhibit the assignment of the ^{11}B spectrum, in this case sufficient observable correlations being present to permit the assignments given in Table 4, which are, in any event, confirmed by the two-dimensional $[^1H-^1H]$-COSY spectra (Figure 5).

There was considerable variation among the intensities of the observed $[^{11}B-^{11}B]$-COSY cross-peaks [Table 4 and structure (**VII**)], for example the long B(5)–B(8) linkage is associated with a particularly weak cross-peak compared to many of the others, as is also observed for the corresponding linkage in $[B_9H_{12}]^-$ and $[B_9H_{11}Cl]^-$ as discussed below. It is likely that the strength of these off-diagonal correlations, as well as their incidences, will have increasing diagnostic value in the general case.* It is also apparent that the presence of the metal centre induces variations in the strengths of these correlations in the *nido* nine-vertex cluster. Thus the B(7)–B(8) correlation is strong, whereas in $[B_9H_{12}]^-$ (Table 6) the corresponding B(7)–B(6)B(8) correlation is weak. The possible (though very weak) longer-range correlation between the 3 and 8 positions is also noteworthy because this would imply a magnitude of a few Hz for the $^2J(^{11}B-^{11}B)$, a coupling rarely observed to date in polyhedral boron chemistry.

The two-dimensional $[^1H-^1H]$-COSY technique (Figure 5) has only recently been applied to polyhedral borane structures.[12,13] The strength of the observed $^1H-^1H$ correlations

* It should be noted that the observation of $[^{11}B-^{11}B]$-COSY correlations will depend upon $T_2^*(^{11}B)$ as well as $^nJ(^{11}B-^{11}B)$ so that caution is required in the comparison of results among compounds of different molecular bulk, or compounds for which COSY data have been measured under different solution conditions.

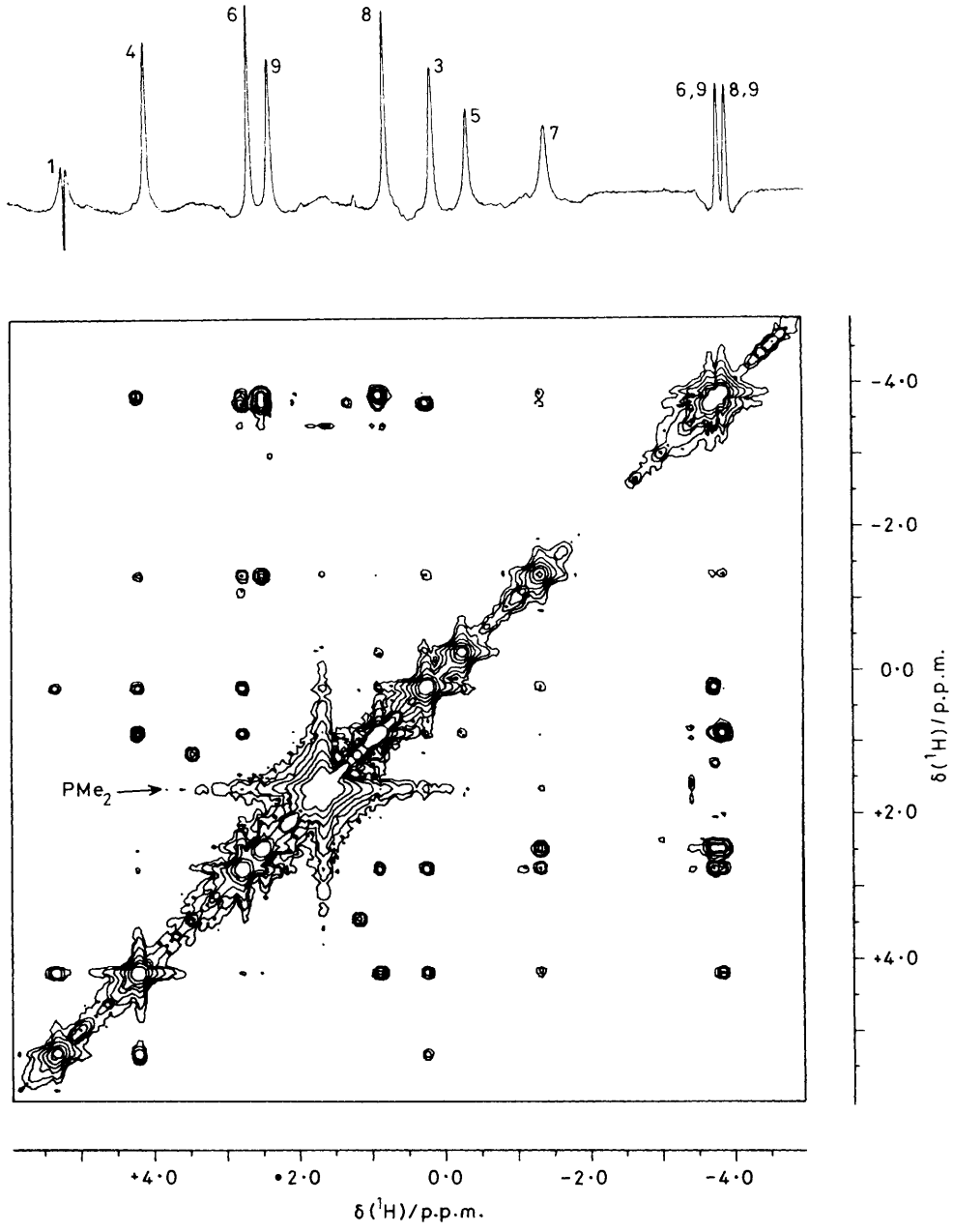

Figure 5. 400-MHz ^{1}H-{^{11}B (broad-band noise)} N.m.r. spectra for $[(PMe_2Ph)_3H_2ReB_8H_{11}]$ (**2**) in CD_2Cl_2 solution at 294 K: the uppermost trace is a straightforward 'one-dimensional' spectrum from which an otherwise equivalent ^{1}H-{^{11}B(broad-band noise, off-resonance)} spectrum has been subtracted; the inverted resonance feature coincident with ^{1}H(1) arises from a partially saturated CH_2Cl_2 resonance. Bridging proton [at $\delta(^1H)$ −14.09 p.p.m.] and Re–^{1}H(terminal) resonances are not included for clarity of scale. The bottom diagram is a (symmetrized) homonuclear two-dimensional COSY-90 contour plot, the large resonance on the diagonal arising from the PMe_2Ph alkyl protons

among *exo*-terminal proton resonances depends upon the magnitudes of the various couplings $^3J(^1H–B–B–^1H)$, which can be up to some 15 Hz or so.[6,31] For bridging (and *endo*-terminal) hydrogen atoms there will in addition be correlations arising from couplings $^2J(^1H–B–^1H)$ which can take similar magnitudes,[6,16,31,32] and correlations from certain $^4J(^1H–B–B–B–^1H)$ paths are also occasionally apparent. [It may be noted that the descriptor *n* in $^nJ(XY)$ does not necessarily imply *n* two-electron two-centre bonds in 'electron-deficient' polyhedral compounds such as the metallaboranes.[6,13,33,34]] The correlations are ideally observed under conditions of complete {^{11}B(broad-band noise)} decoupling,[12,13] the principal practical difficulty being the ensurance of complete decoupling when the ^{11}B spectrum covers a large chemical shift range (see footnotes *e* and *g* to Tables 4 and 6 respectively). As with the $^{11}B–^{11}B$ correlations, there is significant variation among the relative strengths of the observed correlations [see Figure 5 and structure (**VIII**)], these presumably reflecting the magnitudes of the couplings $^nJ(^1H–^1H)$, and sufficient correlations are apparent to assign the spectrum, particularly in conjunction with the [$^{11}B–^{11}B$]-COSY work so that, *via* ^{1}H-{^{11}B(selective)} spectroscopy, assignments from both types of experiment are mutually interconfirmed. The ^2J and ^3J correlations involving the bridging protons are particularly

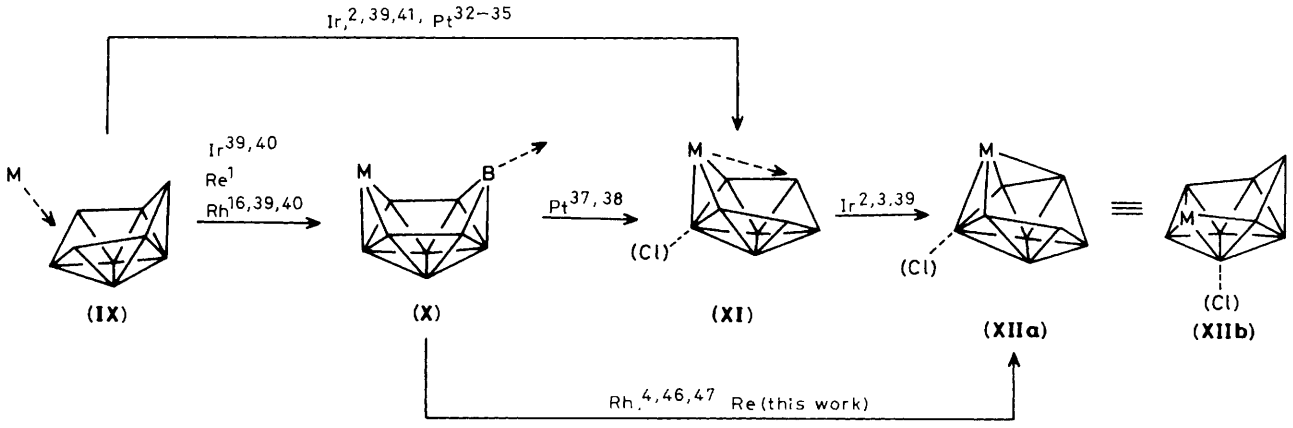

Scheme.

Table 5. Proton and phosphorus-31 n.m.r. data for bridging and rhenium-bound hydrogen and phosphorus atoms in $[(PMe_2Ph)_3H_2ReB_8H_{11}]$ in CD_2Cl_2 solution[a]

Proton data	
$\delta(^1H)[ReH(2b)]_{278}$[b]	−4.78 p.p.m.;[c–e] 1:1 doublet, splitting 51 Hz, of 1:2:1 triplets, splitting 39 Hz, implying one coupling $^2J(^{31}P\text{–}Re\text{–}^1H)$ of *ca.* 51 Hz, and two couplings $^2J(^{31}P\text{–}Re\text{–}^1H)$ of *ca.* 39 Hz
$\delta(^1H)[ReH(2a)]_{278}$[b]	−9.12 p.p.m.;[c–e] approximately 1:2:1 triplet, splitting *ca.* 32 Hz, implying two couplings $^2J(^{31}P\text{–}Re\text{–}^1H)$ of approximately this magnitude and one *ca.* 0
$\delta(^1H)[H(2,5)]_{278}$	−14.32 p.p.m.;[e] doublet structure, implying one coupling $^2J(^{31}P\text{–}Re\text{–}^1H)$ *ca.* 26 Hz; additional fine structure, removed in $^1H\text{-}\{^{31}P\}$ experiments, suggests other two $^2J(^{31}P\text{–}Re\text{–}^1H)$ values *ca.* 5 Hz
$\delta(^1H)[H(6,9)$ and $H(8,9)]_{294}$	−3.81[e] and −3.89[e] p.p.m.
Phosphorus-31 data[d]	
$\delta(^{31}P)_{223}$[f]	A, −27.5; B, −30.9; C, −35.1 p.p.m.

$^2J(^{31}P_A\text{–}^{31}P_B)_{223}$ 11 ± 1; $^2J(^{31}P_B\text{–}^{31}P_C)_{223}$ 11 ± 1; $^2J(^{31}P_A\text{–}^{31}P_C)_{223}$ 20 ± 1 Hz

[a] Temperatures indicated as subscripts. [b] Correspondence between H(2a) and H(2b) here and those in structure (**VI**) and Figure 1 is only tentative. [c] Resonances $\delta(^1H)$ −4.78 and −9.12 p.p.m. coalesce at 343 K (400 MHz), giving $\Delta G^{\ddagger}_{343}$ *ca.* 61 kJ mol^{-1} for the exchange process (compare footnote *f*). [d] Low-temperature experiments showed no evidence for a multi-stage fluxionality with $^{31}P_3{}^1H_2$ sub-spectra corresponding to those observed for $[(PMe_2Ph)_3HReB_9H_{13}]$ and $[(PMe_2Ph)_3H_2WB_9H_{13}]$ (refs. 1, 11, and 35). [e] At higher temperatures (*e.g.* 373 K) a general broadening of resonances for MH, MHB, and BHB was observed, possibly indicative of incipient exchange of MH and MHB accompanied by exchange also with BHB (compare $[B_9H_{12}]^-$ and $[B_9H_{11}Cl]^-$). A general decomposition at these higher temperatures precluded further investigation. [f] Coalescence of these three resonances occurred at *ca.* 313 K (40.25 MHz), giving $\Delta G^{\ddagger}_{313}$ *ca.* 60 kJ mol^{-1} for the exchange process (compare footnote *c*).

useful, and the incidence of some longer-range couplings, of which the 'W-path' $^1H(6)\text{–}^1H(8)$ correlation is particularly noticeable, is also of interest.

The observed ^{31}P and ^1H n.m.r. properties of the $ReH_2(PMe_2Ph)_3$ exopolyhedral co-ordination subsphere and of the cluster bridging hydrogen atoms are summarised in Table 5. At low temperatures two different Re–H(terminal) and three different phosphine resonances are apparent, in accord with the molecular asymmetry (Figure 1). With an increase in temperature the three ^{31}P resonances broaden and then mutually coalesce, the coalescence temperature (at 40 MHz) being *ca.* 315 K indicating a mutual exchange process with an approximate activation energy $\Delta G^{\ddagger}$ of *ca.* +60 kJ mol^{-1}. The two Re–H(terminal) proton resonances also mutually coalesce with an increase of temperature ($\Delta G^{\ddagger}$ +61 ± 2 kJ mol^{-1} at 343 K from 400-MHz spectra), showing that the mutual exchange entails a fluxionality of all five bonded centres in the exopolyhedral $ReH_2(PMe_2Ph)_3$ co-ordination subsphere. This compares with a fluxionality of the $WH_2(PMe_2Ph)_3$ and $ReH(PMe_2Ph)_3$ co-ordination subspheres in the ten-vertex *nido*-6-metalladecaboranes $[(PMe_2Ph)_3H_2WB_9H_{13}]$[11,35] and $[(PMe_2Ph)_3HReB_9H_{13}]$[1] respectively, in both of which a multi-stage fluxionality, involving the successive incorporation of different subsets of ligands, appears to occur, although there is no evidence for such a multiple-stage process in the nine-vertex *nido*-2-rhenaborane described in this work. At higher temperatures ($\geqslant$ *ca.* 380 K), however, there is some broadening of the coalesced ReH_2 proton resonance, the Re–H–B resonance, and the two B–H–B resonances, but it is not possible to ascertain whether this represents an incipient rapid exchange of the three bridging hydrogen atoms (compare the $[B_9H_{11}Cl]^-$ anion, near Table 6 below), possibly also involving the ReH_2 terminal hydrogen atoms (compare $[OsH_3(BH_4)\{P(C_5H_9)_3\}]$[36] and $[(PMe_2Ph)_3H_2WB_9H_{13}]$)[35], because at these temperatures a general decomposition of the compound commences.

(*d*) *Mechanistic Pathways and N.M.R. Properties of the* nido-$[B_9H_{11}Cl]^-$ *Anion.*—The degradation of the *nido* ten-vertex 6-rhenadecaborane (**1**) to give the nine-vertex *nido* species (**2**) [section (*a*) above], and the definitive assignment of the chloro substituent in the iridaborane cluster of $[(CO)(PMe_3)_2IrB_8H_{10}Cl]$ to the 3 position [section (*c*) above], suggest a possible mechanistic pathway (Scheme) in which a metal centre attacks the *arachno* nine-vertex nine-boron substrate [structure (**IX**)] ultimately to give a *nido* nine-vertex eight-boron one-metal product [structures (**XII**)]. This proceeds initially *via* a *nido* ten-vertex species (**X**) which loses a vertex to give an *arachno* nine-vertex metal-containing species (**XI**), and this then closes to give the *nido*-2-metallanonaborane product (**XII**). It is probable that in some systems the open ten-vertex intermediate (**X**) will have some *arachno* character particularly in a transition state to (**XI**): for example, *arachno*-type ten-vertex species such as $[(PMe_2Ph)_2PtB_9H_{11}(PMe_2Ph)]$ readily lose the ligand-substituted boron vertex to give the nine-vertex species $[(PMe_2Ph)_2PtB_8H_{12}]$ of configuration (**XI**).[37,38]

Table 6. Boron-11 and proton n.m.r. data for the *nido* nine-vertex anions $[B_9H_{12}]^-$ and $[B_9H_{11}Cl]^-$, examined as $[NEt_4]^+$ salts in saturated CD_2Cl_2 solution [at +21 °C (294 K) except where otherwise stated]

Assignment[a]	$\delta(^{11}B)$[b]	Observed $[^{11}B-^{11}B]$-COSY correlations[c,d]	$^1J(^{11}B-^1H)$[e]/Hz	$\delta(^1H)$[f]	Observed $[^1H-^1H]$-COSY correlations[c,g,h]
$[B_9H_{11}Cl]^-$					
1	−13.6	(2)s, (5)s, (3)s, (4)/(8)[k]	*ca.* 150	+2.58	(2)s, (4)m, (5)s, μ(2,5)m
2	−33.6	(1)s, (3)s, (6)w	151	+1.36	(1)s, (4)m_4, μ(2,5)m_2 (see footnote *g*)
5	−38.3	(1)s, (4)/(8)[k]	151	+0.48	(1)s, (4)w?, (8)w, μ(2,5)s_2 (see footnote *g*)
3	+1.9[m]	(1)s, (2)s, (4)/(8),[k] (6)s, (7)w	*m*	*m*	*m*
4	*ca.* −7.9[k]	[(1), (3), (5), (7)][k]	*ca.* 140	+2.20	(1)m, (2)m_4, (5)w?, (7)m, μ(2,5)w?, μ(8,9)w?
6	−15.4	(2)w, (3)s, (7)w, (9)w?	160 ± 30	+1.88	(7)s, (9)w?, μ(6,9)s_2, μ(8,9)m
8	*ca.* −7.9[k]	[(1), (3), (5), (7)][k]	*ca.* 140	+2.04	(4)w?, (5)w, (7)m, μ(6,9)m, μ(8,9)s_2
7	−51.7	(3)w, (4)/(8),[k] (6)w, (9)s	145	−0.76	(4)m, (6)s, (8)m, (9)s (see footnote *g*)
9	−16.5	(6)w?, (7)s	160 ± 30	+2.60	(6)w?, (7)s, μ(6,9)s_2, μ(8,9)s_2
μ(6,9)(bridge)	—	—	< 50	−2.73[o,p]	(6)s_2, (8)m, (9)s_2 (see footnote *q*)
μ(8,9)(bridge)	—	—	< 50	−2.62[o,r]	(6)m, (8)s_2, (9)s_2 (see footnote *q*)
μ(2,5)(bridge)	—	—	< 50	−6.67[o]	(1)m, (2)m_2, (4)w?, (5)s_2 (see footnotes *p* and *q*)

Assignment[a]	$\delta(^{11}B)$[b,i]	Observed $[^{11}B-^{11}B]$-COSY correlations[c,d]	$\delta(^1H)$[f,j]	Observed $[^1H-^1H]$-COSY correlations[c,g,h,j]
$[B_9H_{12}]^-$				
1	[−10.0][l]	[(2)(5)s, (6)(8)m, (7)w][l]	+2.72 (1 H)	(2)(5)s, (3)(4)s, μ(2,5)w
2, 5	−34.2	(6)(8)w, (1)/(3)(4)s[l]	+0.71 (2 H)	(1)s, (3)(4)s, (6)(8)w, μ(6,9)(8,9)w?, μ(2,5)m_2 (see footnote *g*)
3, 4	[−10.0][l]	[(2)(5)s, (6)(8)m, (7)w][l]	+1.68 (2 H)	(1)s, (2)(5)s, (7)s, μ(6,9)(8,9)s, μ(2,5)w (see footnote *n*)
6, 8	−13.9	(1)/(3)(4)m,[l] (2)(5)w, (7)w?	+1.72 (2 H)	(2)(5)w, (7)s, μ(6,9)(8,9)m_2 (see footnote *n*)
7	−52.0	(1)/(3)(4)w,[l] (6)(8)w, (9)s	0.94 (1 H)	(3)(4)s, (6)(8)s, (9)s, μ(6,9)(8,9)m (see footnote *g*)
9	−14.5	(7)s	+2.60 (1 H)	(7)s, μ(6,9)(8,9)s_2
μ(6,9)(bridge), μ(8,9)(bridge)	—	—	−2.96 (2 H)[s]	(3)(4)s, (6)(8)m_2,(7)m, (9)s_2, μ(2,5)w?
μ(2,5)(bridge)	—	—	−7.14 (1 H)[s]	(1)w, (2)(5)m_2, (3)(4)w, μ(6,9)(8,9)w?

[a] Numbering as in structure (**III**). [b] δ(^{11}B) in p.p.m. ±0.5 to high frequency (low field) of Ξ 32 031 971 Hz [nominally $BF_3(OEt_2)$ in $CDCl_3$ solution; ref. 6]. [c] Observed correlations under the conditions stated are designated stronger (s), weaker (w), or intermediate (m). [d] The strength of the observed correlation will depend upon solution conditions as well as upon the interboron coupling constants (see refs. 6, 16, and 34). [e] Measured from ^{11}B spectrum with line narrowing to give baseline separation of doublet components. [f] δ(^{1}H) in p.p.m. to high frequency (low field) of Ξ 100 (nominally internal $SiMe_4$) using solvent residual ^{1}H resonances as secondary standard; ^{1}H resonances related to directly bound B positions by ^{1}H-{^{11}B(selective)} spectroscopy. [g] Obtained under ^{1}H-{^{11}B(broad-band noise)} conditions; some correlations for ^{1}H(2), ^{1}H(5), and ^{1}H(7) may be weaker or not observed because of the impossibility of achieving simultaneous complete decoupling of all ^{11}B resonances on the equipment available. [h] Numerical subscripts refer to value of *n* in $^nJ(^1H-^1H)$ when $n \neq 3$; note that in polyhedral chemistry *n* does not necessarily imply *n* two-electron two-centre bonds (see refs. 6 and 33). [i] Very recent reports[7,59] contain some related ^{11}B n.m.r. data on the $[B_9H_{12}]^-$ anion; the work is essentially in agreement with the results presented here (see also Table 7 in ref. 3). [j] Values for 228 K. Higher dispersion at 9.4 T together with $[^1H-^1H]$-COSY correlations remove ambiguities from work at 2.35 T previously reported.[3] [k] Resonances for ^{11}B(4) and ^{11}B(8) accidentally coincident. [l] Resonances for ^{11}B(1) and ^{11}B(3)(4) accidentally coincident. [m] Chlorine-substituted position. [n] Some (unobserved) correlations with ^{1}H(2) may have been obscured by coincident ridge effects from strong counter-cation resonances. [o] At 243 K; at ambient temperatures there is rapid exchange among these sites, with $\Delta G^‡$ 50.5 ± 2.5 kJ mol^{-1} at 249 and 283 K. [p] Selectively decoupled by ν[^{11}B(6)] in selective ^{1}H-{^{11}B} experiments. [q] Experiments to observe correlations with bridging protons carried out at 213 K. [r] Not selectively decoupled by ν[^{11}B(6)] in selective ^{1}H-{^{11}B} experiments. [s] At ambient temperatures there is rapid exchange between these two bridging-site types, $\Delta G^‡$ 52 kJ mol^{-1} at 279 K (ref. 3).

Variations in the constituents of and the substituents on the metallaborane clusters will stabilise particular minima on the reaction co-ordinate of the Scheme. For the reaction of some metal substrates, for example $[IrCl(PPh_3)_3]$,[39,40] $[\{Rh(cod)Cl\}_2]$ (cod = cyclo-octa-1,5-diene),[39,40] $[ReCl_3(PMe_2Ph)_3]$,[1] and $[\{Rh(C_5Me_5)Cl_2\}_2]$,[16] with the *arachno*-$[B_9H_{14}]^-$ anion (**IX**), a geometrically straightforward addition of the metal centre to the cluster, to give a 6-metalla *nido* ten-vertex structure (**X**), occurs. With $[Ir(CO)Cl(PPh_3)_2]$[2,39,41] and $[PtCl_2(PMe_2Ph)_2]$,[42,43] however, the predominant process is the formation of *arachno* nine-vertex species of configuration (**XI**), and recently reported labelling experiments on the platinum system indicate that this occurs *via* an initial attack by the metal as in (**IX**) followed by elimination of the opposing vertex, marked as 'B' in structure (**X**).[44,45] The *arachno* iridaborane $[(CO)(PMe_3)_2HIrB_8H_{11}Cl]$ of configuration (**XI**) readily thermolyses to give $[(CO)(PMe_3)_2IrB_8H_{10}Cl]$ of *nido* configuration (**XII**),[2,3,39] and the 3-Cl assignment for this latter established in section (*c*) above confirms that these *nido*-2-iridanonaboranes result from a straightforward *arachno* ⟶ *nido* geometrical closure[3] as indicated by the hatched lines in structure (**XI**). This in turn suggests that the degradation of the *nido*-6-rhenadecaborane (**1**) [configuration (**X**)] to give the *nido*-2-rhenanonaborane (**2**) [equations (1) and (2)] also occurs *via* 9-boron vertex loss and an *arachno* intermediate of configuration (**XI**) which undergoes closure to give the product configuration (**XII**). This may occur in a concerted fashion, the process being related to a geometrically analogous phosphine-induced closure

of [6-(C_5Me_5)-*nido*-6-RhB_9H_{13}] to give [2-(C_5Me_5)-*nido*-2-RhB_8H_{10}-6-(PMe_2Ph)] as reported elsewhere.[4,46]

The variations among different metal centres as regards behavioural type reflect their differing ability to act as electron sinks or donors, and/or as sites of bonding flexibility to accommodate or prevent cluster transition states or transition states for hydrogen atoms as they move about the open face during the reaction processes. Also it should be emphasized that in certain systems other reactions can compete with the processes in the Scheme. For example, the ten-vertex *nido*-6-metalladecaborane configuration (**X**) can isomerise *via* a swing of atom B to give a *nido*-5-metalladecaborane,[4,30,39,46–48] and there is also an extensive chemistry of cluster closures in this area[48] to give *closo*,[4,49–51] *isocloso*,[20,39,52,53] and *isonido*[39,49,54] ten-vertex configurations. Likewise the *arachno* platinanonaboranes of configuration (**XI**) undergo *aufbau* processes to give macropolyhedral clusters of fourteen,[34,43,45] seventeen,[34] and eighteen[55] vertices rather than straightforward cluster closure to give *nido*-type structures of configuration (**XII**), and reactions to give *arachno* iridaboranes of configuration (**XI**) are accompanied by cluster degradation reactions to yield iridaboranes of five vertices and fewer.[39,48,56]

It is of interest to compare the closure process (**XI**) ⟶ (**XII**) in the Scheme to give a nine-vertex *nido*-metallaborane with the related binary borane closure reaction of *arachno*-$B_9H_{13}(SMe_2)$ with alcoholic hydroxide to give the *nido*-$[B_9H_{12}]^-$ anion.[45,57] The mechanism of this latter process has not received attention since the excellent and meticulous labelling work of Siedle *et al.*[58] over a decade ago, for which the interpretation of results was rendered difficult because the ^{11}B n.m.r. spectrum of *nido*-$[B_9H_{12}]^-$ had not then been assigned. Selective ^1H-{^{11}B}, two-dimensional [^{11}B–^{11}B]-COSY, and two-dimensional [^1H–^1H]-COSY n.m.r. experimentation now permits the unambiguous assignment of the ^{11}B and ^1H parameters as summarised in Table 6 (see also refs. 3, 7, and 59). Inspection of the n.m.r. spectra reported by Siedle *et al.* for the tetradeuteriated *nido* anion $[B_9H_8D_4]^-$ that they obtained by closure of the 1,2,3,7 tetradeuteriated 4-(SMe_2)-substituted *arachno* precursor $B_9H_{13}(SMe_2)$ thence readily shows that their $[B_9H_8D_4]^-$ product is deuteriated at the 3,4,6,7 positions, these four boron positions being indicated by the heavier connecting lines in the schematic structures of equation (3) [for numbering schemes see structures (**II**) and (**III**) in the Introduction].

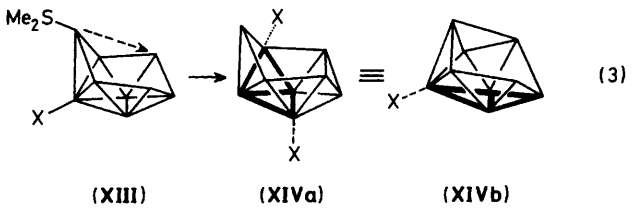

(**XIII**) (**XIVa**) (**XIVb**) (3)

It can be seen that the tetradeuteriated four-boron diamond is retained, the only unanswered question in the gross skeletal closure then being that of any effective rotation of the four-boron diamond within the cluster, *i.e.* will a substituent at the 1 position on a species 1-X-$B_9H_{12}(SMe_2)$ [structure (**XIII**)] end up at the 3/4 position in $[B_9H_{11}X]^-$ [hatched lines in structures (**XIVa**) and (**XIVb**)] or at the 6/8 position [dotted lines in structure (**XIVa**)]? This is resolved by selective ^1H-{^{11}B} and two-dimensional [^{11}B–^{11}B]-COSY n.m.r. experiments on the substituted *nido* anion $[B_9H_{11}Cl]^-$ that is obtained by closure from *arachno*-1-Cl-B_9H_{12}-4-(SMe_2).[45,58,60] This n.m.r. work (Table 6 and Figure 6) assigns the spectra of the anionic species, and specifically the chloride substituent is thereby shown to be at the 3 position [hatched lines in structures (**XIVa**) and (**XIVb**), X = Cl]. This indicates that a straightforward closure

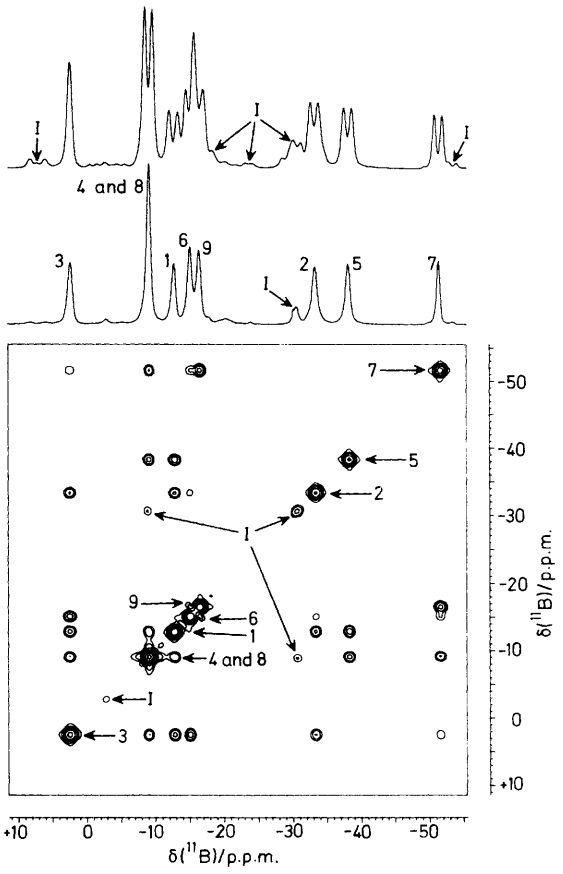

Figure 6. 128-MHz ^{11}B N.m.r. spectra for $[B_9H_{11}Cl]^-$: the top trace is the normal ^{11}B spectrum, the centre trace is the ^{11}B-{^1H-(broad-band noise)} spectrum, and the bottom diagram is a (symmetrized) homonuclear two-dimensional COSY-90 contour plot from data acquired under conditions of {^1H(broad-band noise)} decoupling; I = principal impurity peaks. The top spectrum was recorded sometime after the centre one and exhibits increased impurities arising from decomposition of the compound

of B(4) with B(8)B(9) has occurred in the *arachno* species [hatched arrow in structure (**XIII**)] to give the *nido* product (**XIV**) (X = Cl). This perhaps occurs *via* an effective deprotonation at the B(8)–H–B(9) bridge site of the *arachno* compound followed by an effective internal nucleophilic displacement of SMe_2 at B(4) by the resulting or incipient anionic B(8)–B(9) two-centre two-electron configuration. The geometry of the closure reaction is thus seen to be similar to that proposed for the formation of the nine-vertex *nido*-2-metallanonaboranes discussed above.

Points of interest in this n.m.r. work itself include the high nuclear shieldings associated with the open-face boron atoms B(2) and B(5) together with their bridging hydrogen atom H(2,5),[59] and the observation of fluxionality resulting in the mutual exchange of the three bridging hydrogen positions of $[B_9H_{11}Cl]^-$, for which the activation energy $\Delta G^{\ddagger}$ from n.m.r. coalescence temperatures was found to be *ca.* + 50.5 kJ mol^{-1} at 249 and 283 K. This value is essentially the same, within experimental error, as the value of *ca.* 52 kJ mol^{-1} at 279 K previously found by Bould *et al.*[3] for the unsubstituted parent $[B_9H_{12}]^-$. Again there is a general parallel in nuclear shielding between the cluster boron atoms and their directly bound *exo*-hydrogen atoms (Figure 7), as has been observed for a variety of other polyhedral boron-containing species,[4,6,11,28,34,43] including the metallaboranes discussed above (Figure 2). In the ^{11}B

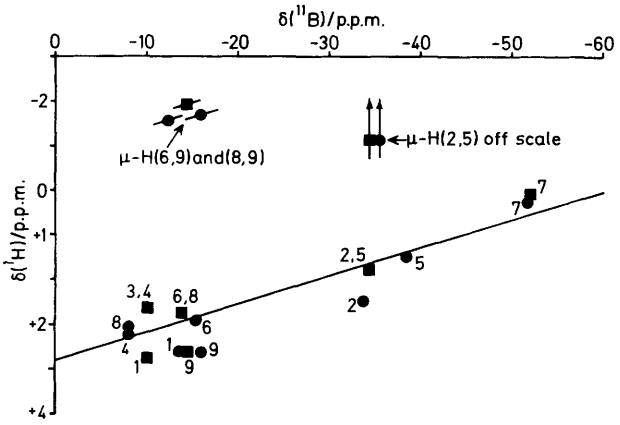

Figure 7. Proton-boron-11 shielding correlation plot [$\delta(^1H)$ *versus* $\delta(^{11}B)$] for the *nido* anions $[B_9H_{12}]^-$ (■) and $[3\text{-}ClB_9H_{11}]^-$ (●). The H(2,5) bridging protons are anomalously highly shielded and are off-scale to negative $\delta(^1H)$. The line drawn has slope $\delta(^1H):\delta(^{11}B)$ of 1:16, intercept $\delta(^1H) = +2.75$ p.p.m.

n.m.r. spectrum it is of interest that the α-deshielding effect of the chlorine substituent on B(3) is relatively small, with $\Delta\sigma$ *ca.* −12 p.p.m., and it is of interest that variations between some of the β and γ effects (which have $\Delta\sigma$ in the range −5.0 to +4.1 p.p.m.) are nearly of comparable magnitudes.

In the two-dimensional [^{11}B–^{11}B]-COSY n.m.r. work on the two anions noteworthy points include (*a*) the weak or effectively absent correlations observed for the open-face B–H–B bridged positions and for the long B(2)–B(6) and B(5)–B(8) linkages, as also observed in *nido* ten-vertex species,[4,6,12–16,30] and (*b*) the stronger correlations B(7)–B(9) allied with the much weaker ones from B(7) to B(6) and B(8), again mirrored in the comparable correlations for B(2) [or B(4)] in ten-vertex *nido* compounds [numbering as in structures (**I**) and (**II**)].[4,6] Also of interest are (*c*) the strong correlations between B(1) and all of its four circumjacent boron atoms, as is also often observed for the axial boron atoms in the few bicapped square-antiprismatic *closo* structures that have so far been investigated by two-dimensional [^{11}B–^{11}B]-COSY n.m.r. spectroscopy,[4,12–15,61] again emphasising bonding parallels with *closo* ten-vertex clusters in this region of the *nido* nine-vertex molecule as mentioned above for the metallaboranes.

As mentioned above, the [^1H–^1H]-COSY technique has only recently been applied to polyhedral boranes,[12,13] and the results for $[B_9H_{12}]^-$ and $[B_9H_{11}Cl]^-$ (also in Table 6) consequently merit some comment. As with the rhenaborane (**2**) (Table 4), therefore, there is considerable variation among the strengths of the various correlations within and between $[B_9H_{12}]^-$ and $[B_9H_{11}Cl]^-$ [with due allowance for inefficient $\{^{11}B\}$ decoupling of the extreme ^{11}B resonances of B(8), B(5), and B(7)]. In particular it is noteworthy that there are only weak correlations for each of the *exo*-terminal proton pairs (2)(5), (2)(6), (5)(8), (6)(9), and (8)(9), mirroring the behaviour of the corresponding interboron couplings $^1J(^{11}B$–$^{11}B)$ mentioned in the previous paragraph, and also mirroring the behaviour of both interproton and interboron correlations in ten-vertex *nido* systems.[12–16]

In general the [^1H–^1H]-COSY results confirm the connectivities and positional assignments obtained from the [^{11}B–^{11}B]-COSY plot [the ^1H resonances being directly relatable to their directly bound boron positions by ^1H-$\{^{11}B$(selective)$\}$ spectroscopy] and they also permit some minor ambiguities to be resolved. These last include in particular the assignment of the resonances at $\delta(^1H)$ +2.20 and +2.04 p.p.m. between $^1H(4)$ and $^1H(8)$ in $[B_9H_{11}Cl]^-$ [not possible from ^1H-$\{^{11}B\}$ spectroscopy because of the accidental coincidence of the $^{11}B(4)$ and $^{11}B(8)$ resonances], and also the confirmation of the $^1H(6,9)$ and $^1H(8,9)$ bridging-proton resonance assignments using both $^2J(^1H$–$^1H)$ and $^3J(^1H$–$^1H)$ correlations. An interesting observation is the *trans* cluster coupling $^4J[^1H(2)$–$^1H(4)]$ in $[B_9H_{11}Cl]^-$: this occurs across the base of the B(1)B(2)B(3)B(4)B(5) square-pyramidal 'cap,' and may have some diagnostic use for this feature in the general case [compare antipodal '^5J(X–B–B–B–B–Y)' couplings in icosahedral systems].[13] However, a similar correlation was not observed for the rhenaborane (**2**) (Table 4) and conversely the correlations arising from $^4J[^1H(6)$–B–B–B–$^1H(8)]$ observed in (**2**) were not present in the [^1H–^1H]-COSY plot for $[B_9H_{11}Cl]^-$, illustrative of the pitfalls in the uncritical use of blanket generalisations in polyhedral borane n.m.r. work.[62] It is also salutary that there is quite a difference in the relative strengths of many of the ^1H–^1H correlations observed for $[B_9H_{11}Cl]^-$ *versus* $[B_9H_{12}]^-$, showing that the magnitudes of the couplings must be significantly affected by the electronegative chlorine substituent.

Experimental

Preparation of [2,2,2-$(PMe_2Ph)_3$-2,2-H_2-*nido*-2-ReB_8H_{11}] (**2**).—A sample of [6,6,6-$(PMe_2Ph)_3$-6-H-*nido*-6-ReB_9H_{12}-9-(OEt)] (**1**) (55 mg, 0.073 mmol; prepared as in ref. 1) in a n.m.r. tube (outside diameter 10 mm) under N_2 with *sym*-$C_2D_2Cl_4$ (*ca.* 2 cm^3) as solvent was kept at 373 K for 45 min whilst its ^{31}P-$\{^1H$(broad-band noise)$\}$ n.m.r. spectrum at 2.35 T was monitored. The ^{31}P resonance associated with the starting ten-vertex rhenadecaborane (**1**) (δ −16.6 p.p.m. at 373 K)[1] disappeared during this time and was replaced by a new resonance (δ −32.2 p.p.m. at 373 K; see Table 5) which was observed to build up as the resonance associated with the starting material decreased. The volatile components were then evaporated (rotary evaporator, water-bath at *ca.* 360 K, water-pump pressure) and the product isolated by repeated preparative t.l.c. using silica gel (Fluka GF 254; 200 × 200 × 1 mm) as stationary phase, with initially CH_2Cl_2 (100%) [(**2**) as colourless band, R_f 0.8, observed under u.v. illumination] and then diethyl ether–pentane 1:4 [(**2**) as a colourless band, R_f 0.25] as eluting media. This resulted in the isolation of (**2**) as a very pale yellow crystalline solid (44 mg, 0.059 mmol; 81%), characterised as $[(PMe_2Ph)_3H_2ReB_8H_{11}]$ by multielement n.m.r. spectroscopy (Tables 3—5) and single-crystal *X*-ray diffraction analysis of its hemisolvate with CH_2Cl_2 (Tables 1, 2, and 8) as described in the text. Crystals suitable for single-crystal *X*-ray diffraction analysis were obtained by vapour diffusion of diethyl ether into a solution of (**2**) in dichloromethane.

Preparation of $[B_9H_{12}]^-$ *and* $[B_9H_{11}Cl]^-$.—These species were prepared as described in the literature,[45,57,58,60] and examined as the tetramethylammonium salts $[NMe_4][B_9H_{12}]$ and $[NMe_4][B_9H_{11}Cl]$.

N.M.R. Experiments.—These were performed at 2.35 and/or 9.40 T using commercially available instrumentation. The techniques involved in the ^1H-$\{^{11}B\}$,[25,42,63–65] two-dimensional [^{11}B–^{11}B]-COSY,[4,6,16,18] and two-dimensional [^1H–^1H]-$\{^{11}B\}$-COSY[13,22–24] experiments as applied to this work were essentially as described previously. In the ^1H-$\{^{11}B\}$ experiments use was made of the technique[63,65] in which a ^1H-$\{^{11}B$(off-resonance)$\}$ spectrum is subtracted from a ^1H-$\{^{11}B$(on-resonance)$\}$ spectrum in order to eliminate ^1H lines not coupled to the boron nuclei of interest. Parameters used for the two-dimensional COSY experiments are summarised in Table 7. Other n.m.r. spectroscopy was straightforward, initial ^{31}P-

Table 7. Experimental details for two-dimensional experiments

Compound	$[(PMe_2Ph)_3H_2ReB_8H_{11}]$		$[B_9H_{12}]^-$		$[B_9H_{11}Cl]^-$	
Two-dimensional experiment	$[^{11}B-^{11}B]$-COSY	$[^1H-^1H]$-COSY	$[^{11}B-^{11}B]$-COSY	$[^1H-^1H]$-COSY	$[^{11}B-^{11}B]$-COSY	$[^1H-^1H]$-COSY
Data size (t_2,t_1)/words	512, 128	1 024, 256	512, 128	1 024, 128	256, 128	512, 128
Transform size ($F2$,$F1$)/words	1 024, 512	1 024, 512	1 024, 512	1 024, 512	512, 256	512, 256
t_2 sweep width (= 2 × t_1 sweep width)/Hz	7 576	10 204	12 820	4 525	8 620	3 676
Digital resolution ($F2$ and $F1$)/Hz	29.6	19.9	25.0	11.6	33.7	14.4
No. of transients per t_1 increment	512	80	32	32	32	160
Recycling time/s	0.050	2.0	0.05	21.0	0.05	2.0

Mixing pulse 90°. Both dimensions of the time domain matrices were treated by a sine-bell window centred on the centre of the *acquired* data block prior to zero fitting to transform size (*i.e.* a so-called 'unshifted' function; compare D. F. Gaines, G. M. Edvenson, T. G. Hill, and B. R. Adams, *Inorg. Chem.*, 1987, **26**, 1813).

Table 8. Fractional atomic co-ordinates (× 10^4) for compound (**2**) with e.s.d.s in parentheses (see also caption to Figure 1)

Atom	*x*	*y*	*z*	Atom	*x*	*y*	*z*
Re(2)	2 063.7(3)	2 545.6(2)	1 611.5(1)	C(334)	3 547(5)	806(4)	−560(2)
P(1)	1 381(2)	4 185(2)	1 215(1)	C(335)	3 761(5)	1 778(4)	−322(2)
P(2)	354(3)	1 597(2)	1 208(1)	C(336)	3 746(5)	1 904(4)	249(2)
P(3)	3 501(3)	1 283(2)	1 335(1)	B(1)	1 617(11)	1 554(8)	2 308(5)
C(11)	−173(9)	4 515(7)	1 301(5)	B(3)	3 063(11)	2 005(8)	2 464(5)
C(12)	1 462(12)	4 350(7)	478(4)	B(4)	1 906(13)	2 176(9)	2 934(5)
C(131)	2 170(5)	5 334(3)	1 475(2)	B(5)	877(10)	2 714(9)	2 451(5)
C(132)	1 675(5)	6 023(3)	1 837(2)	B(6)	3 515(10)	3 308(8)	2 315(5)
C(133)	2 316(5)	6 889(3)	2 030(2)	B(7)	3 159(10)	3 015(9)	3 004(4)
C(134)	3 453(5)	7 066(3)	1 860(2)	B(8)	1 685(12)	3 506(10)	3 006(5)
C(135)	3 948(5)	6 378(3)	1 498(2)	B(9)	2 935(10)	4 229(8)	2 785(5)
C(136)	3 307(5)	5 511(3)	1 306(2)	Cl(1S)	7 137(6)	3 828(5)	1 913(3)
C(21)	−992(9)	1 510(9)	1 578(5)	Cl(2S)	6 345(6)	4 655(5)	859(3)
C(22)	569(10)	224(7)	1 056(5)	C(1S)	6 480(20)	4 591(17)	1 524(10)
C(231)	−239(6)	2 001(4)	517(2)	H(1)	1 174(34)	710(33)	2 314(25)
C(232)	466(6)	1 873(4)	72(2)	H(3)	3 882(34)	1 494(33)	2 469(25)
C(233)	30(6)	2 153(4)	−460(2)	H(4)	1 627(33)	1 798(31)	3 453(23)
C(234)	−1 112(6)	2 560(4)	−548(2)	H(5)	−118(35)	2 773(32)	2 434(25)
C(235)	−1 817(6)	2 687(4)	−104(2)	H(6)	4 560(35)	3 411(33)	2 199(26)
C(236)	−1 380(6)	2 408(4)	429(2)	H(7)	3 809(33)	2 862(31)	3 333(24)
C(31)	5 043(9)	1 697(8)	1 478(4)	H(8)	1 130(34)	3 761(32)	3 331(25)
C(32)	3 537(10)	−13(7)	1 624(4)	H(9)	3 313(33)	4 971(32)	2 930(24)
C(331)	3 517(5)	1 058(4)	583(2)	H(6,9)	2 968(35)	4 212(33)	2 296(27)
C(332)	3 303(5)	86(4)	345(2)	H(8,9)	1 781(35)	4 284(34)	2 758(27)
C(333)	3 318(5)	−40(4)	−226(2)				

$\{^1H$(broad-band noise)$\}$ experiments being conducted at low temperatures in order to maximise 'thermal decoupling' of the ^{10}B and ^{11}B nuclei [$^2J(^{31}P$–Re–$^{11}B)$ (estimated) up to *ca.* 30 Hz].[6,63] Chemical shifts $\delta(^1H)$, $\delta(^{31}P)$, and $\delta(^{11}B)$ are given in p.p.m. to high frequency (low field) of Ξ100 ($SiMe_4$), Ξ40.480 730 (nominally 85% H_3PO_4), and Ξ32.083 971 MHz [nominally $BF_3(OEt_2)$ in $CDCl_3$] respectively.

X-*Ray Crystallographic Studies.*—All crystallographic measurements were made on a Syntex $P2_1$ diffractometer operating in the ω–2θ scan mode using graphite-monochromated Mo-K_α radiation (λ = 71.069 pm) following a procedure described in detail elsewhere.[66] The data set was corrected for absorption empirically[67] after the structure had been solved.

The structure was solved *via* standard heavy-atom methods and refined by full-matrix least squares using the SHELX program system.[68] All non-hydrogen atoms (excluding a CH_2Cl_2 solvent molecule, refined with an occupancy factor of 0.5 and an overall isotropic thermal parameter) were assigned anisotropic thermal parameters. All phenyl groups were included in refinement as rigid bodies with hexagonal symmetry (C–C 139.5 pm). All phenyl and methyl hydrogen atoms were included in calculated positions (C–H 108 pm) and refined with an overall isotropic thermal parameter for each phosphine group. All other borane hydrogen atoms (except those attached to the rhenium atom which were not located) were located experimentally and refined freely with individual isotropic thermal parameters. The weighting scheme $w = [\sigma^2(F_o) + g(F_o)^2]^{-1}$ was applied with the parameter g included in the refinement so as to give a flat analysis of variance with increasing sin θ and $(F/F_{max.})^{\frac{1}{2}}$. Non-hydrogen and hydrogen atom co-ordinates are in Table 8.

Additional material available from the Cambridge Crystallographic Data Centre comprises H-atom co-ordinates, thermal parameters, and remaining bond distances and angles.

Crystal data. $C_{24}H_{46}B_8P_3Re{\cdot}0.5CH_2Cl_2$, M = 742.71, monoclinic, a = 1 130.0(3), b = 1 292.2(3), c = 2 424.0(5) pm, β = 94.15(2)°, U = 3.530 nm^3, space group $P2_1/c$, Z = 4, D_c = 1.397 g cm^{-3}, μ(Mo-K_α) = 34.96 cm^{-1}, $F(000)$ = 1 484.

Data collection parameters. Scans running from 1° below $K_{\alpha 1}$ to 1° above $K_{\alpha 2}$, scan speeds 2.0—29.3° min^{-1}, 4.0 ≤ 2θ ≤ 45.0°.

3 995 Unique data, 3 516 observed [$I > 2.0\sigma(I)$], $T = 290$ K.

Structure refinement. Number of parameters = 360, weighting factor $g = 0.0004$, $R = 0.0399$, $R' = 0.0454$.

Acknowledgements

We thank the S.E.R.C. for support, and the University of Leeds Research Fund for a grant (to J. D. K. and M. T-P.).

References

1 M. A. Beckett, N. N. Greenwood, J. D. Kennedy, and M. Thornton-Pett, *J. Chem. Soc., Dalton Trans.*, 1985, 1119.
2 J. Bould, J. E. Crook, N. N. Greenwood, J. D. Kennedy, and W. S. McDonald, *J. Chem. Soc., Chem. Commun.*, 1982, 346.
3 J. Bould, N. N. Greenwood, and J. D. Kennedy, *J. Chem. Soc., Dalton Trans.*, 1984, 2477.
4 X. L. R. Fontaine, H. Fowkes, N. N. Greenwood, J. D. Kennedy, and M. Thornton-Pett, *J. Chem. Soc., Dalton Trans.*, 1987, 1431.
5 H. Nöth and B. Wrackmeyer, 'Nuclear Magnetic Resonance Spectroscopy of Boron Compounds,' Springer, Berlin, Heidelberg, and New York, 1978.
6 J. D. Kennedy, in 'Multinuclear NMR,' ed. J. Mason, Plenum, London and New York, 1987, ch. 8, pp. 221—258 and refs. cited therein (A preliminary title for this book was 'NMR in Inorganic and Organometallic Chemistry,' and it is so cited in refs. 1, 3, and 43).
7 G. B. Jacobsen, D. G. Meina, J. H. Morris, C. Thompson, S. J. Andrews, D. Reed, A. J. Welch, and D. F. Gaines, *J. Chem. Soc., Dalton Trans.*, 1985, 1645.
8 J. D. Kennedy, A. G. Orpen, and M. Thornton-Pett, unpublished work.
9 A. G. Orpen, HYDEX and XHYDEX programs for indirect H atom location using potential-well calculations; see also, A. G. Orpen, *J. Chem. Soc., Dalton Trans.*, 1980, 2509.
10 C. H. Schwalbe and W. N. Lipscomb, *Inorg. Chem.*, 1971, **10**, 160.
11 M. A. Beckett, N. N. Greenwood, J. D. Kennedy, and M. Thornton-Pett, *J. Chem. Soc., Dalton Trans.*, 1986, 795.
12 X. L. R. Fontaine, results presented to the Fifth National Meeting of British Inorganic Boron Chemists, INTRABORON 5, Edinburgh/Killin, September 1985.
13 X. L. R. Fontaine and J. D. Kennedy, *J. Chem. Soc., Chem. Commun.*, 1986, 779.
14 T. L. Venable, W. C. Hutton, and R. N. Grimes, *J. Am. Chem. Soc.*, 1984, **106**, 29.
15 D. Reed, *J. Chem. Res.(S)*, 1984, 198.
16 X. L. R. Fontaine, H. Fowkes, N. N. Greenwood, J. D. Kennedy, and M. Thornton-Pett, *J. Chem. Soc., Dalton Trans.*, 1986, 547.
17 X. L. R. Fontaine, H. Fowkes, N. N. Greenwood, J. D. Kennedy, and M. Thornton-Pett, *J. Chem. Soc., Chem. Commun.*, 1985, 1165, 1722.
18 X. L. R. Fontaine, H. Fowkes, N. N. Greenwood, J. D. Kennedy, and M. Thornton-Pett, *J. Chem. Soc., Dalton Trans.*, 1987, 2417.
19 X. L. R. Fontaine, N. N. Greenwood, J. D. Kennedy, P. I. MacKinnon, and M. Thornton-Pett, *J. Chem. Soc., Chem. Commun.*, 1986, 1111.
20 X. L. R. Fontaine, N. N. Greenwood, J. D. Kennedy, I. Macpherson, and M. Thornton-Pett, *J. Chem. Soc., Chem. Commun.*, 1987, 476.
21 M. Bown, X. L. R. Fontaine, N. N. Greenwood, J. D. Kennedy, and P. MacKinnon, *J. Chem. Soc., Chem. Commun.*, 1987, 817.
22 M. Bown, X. L. R. Fontaine, N. N. Greenwood, J. D. Kennedy, and M. Thornton-Pett, *J. Chem. Soc., Dalton Trans.*, 1987, 1169.
23 X. L. R. Fontaine, N. N. Greenwood, J. D. Kennedy, P. I. MacKinnon, and I. Macpherson, *J. Chem. Soc., Dalton Trans.*, 1987, 2385.
24 M. Bown, X. L. R. Fontaine, N. N. Greenwood, J. D. Kennedy, P. I. MacKinnon, and M. Thornton-Pett, *J. Chem. Soc., Dalton Trans.*, 1987, 2781.
25 T. C. Gibb and J. D. Kennedy, *J. Chem. Soc., Faraday Trans. 2*, 1982, 525.
26 D. F. Gaines, C. K. Nelson, J. C. Kunz, J. H. Morris, and D. Reed, *Inorg. Chem.*, 1984, **23**, 3252.
27 J. Bould, N. N. Greenwood, and J. D. Kennedy, *J. Organomet. Chem.*, 1983, **249**, 11.
28 N. N. Greenwood, J. D. Kennedy, M. Thornton-Pett, and J. D. Woollins, *J. Chem. Soc., Dalton Trans.*, 1985, 2397.
29 A. B. Burg, *J. Am. Chem. Soc.*, 1968, **90**, 1407.
30 M. Bown, X. L. R. Fontaine, N. N. Greenwood, and J. D. Kennedy, *J. Organomet. Chem.*, 1987, **325**, 233.
31 J. D. Kennedy, unpublished work.
32 S. K. Boocock, N. N. Greenwood, J. D. Kennedy, W. S. McDonald, and J. Staves, *J. Chem. Soc., Dalton Trans.*, 1980, 790.
33 M. A. Beckett, J. D. Kennedy, and O. W. Howarth, *J. Chem. Soc., Chem. Commun.*, 1985, 855.
34 M. A. Beckett, J. E. Crook, N. N. Greenwood, and J. D. Kennedy, *J. Chem. Soc., Dalton Trans.*, 1986, 1879.
35 M. A. Beckett, X. L. R. Fontaine, and J. D. Kennedy, unpublished work.
36 P. W. Frost, J. A. K. Howard, and J. L. Spencer, *J. Chem. Soc., Chem. Commun.*, 1984, 1362.
37 A. R. Kane, L. J. Guggenberger, and E. L. Muetterties, *J. Am. Chem. Soc.*, 1970, **92**, 2571.
38 Y. M. McInnes, unpublished work.
39 J. Bould, Ph.D. Thesis, University of Leeds, 1983.
40 S. K. Boocock, J. Bould, N. N. Greenwood, J. D. Kennedy, and W. S. McDonald, *J. Chem. Soc., Dalton Trans.*, 1982, 713.
41 J. Bould, J. E. Crook, N. N. Greenwood, and J. D. Kennedy, *J. Chem. Soc., Dalton Trans.*, 1984, 1903.
42 S. K. Boocock, N. N. Greenwood, M. J. Hails, J. D. Kennedy, and W. S. McDonald, *J. Chem. Soc., Dalton Trans.*, 1981, 1415.
43 N. N. Greenwood, M. J. Hails, J. D. Kennedy, and W. S. McDonald, *J. Chem. Soc., Dalton Trans.*, 1985, 953.
44 R. Ahmad, J. E. Crook, N. N. Greenwood, J. D. Kennedy, and W. S. McDonald, *J. Chem. Soc., Chem. Commun.*, 1982, 1019.
45 R. Ahmad, J. E. Crook, N. N. Greenwood, and J. D. Kennedy, *J. Chem. Soc., Dalton Trans.*, 1986, 2433.
46 M. Thornton-Pett, results presented to the 1985 Meeting of the British Crystallography Association, Bristol, March 25—27th, 1985; H. Fowkes, results presented to the Fourth and Fifth National Meetings of British Boron Chemists, INTRABORON 4 and INTRABORON 5, Durham, September 1984, and Killin, September 1985.
47 N. N. Greenwood, *Pure Appl. Chem.*, 1983, **55**, 1415; R. Ahmad, Ph.D. Thesis, University of Leeds, 1982.
48 J. D. Kennedy, *Prog. Inorg. Chem.*, 1984, **32**, 519; 1986, **34**, 211; and refs therein.
49 J. E. Crook, Ph.D. Thesis, University of Leeds, 1982.
50 J. E. Crook, N. N. Greenwood, J. D. Kennedy, and W. S. McDonald, *J. Chem. Soc., Chem. Commun.*, 1983, 83.
51 N. W. Alcock, J. G. Taylor, and M. G. H. Wallbridge, *J. Chem. Soc., Chem. Commun.*, 1983, 1168.
52 J. Bould, N. N. Greenwood, J. D. Kennedy, and W. S. McDonald, *J. Chem. Soc., Chem. Commun.*, 1982, 465.
53 J. E. Crook, M. Elrington, N. N. Greenwood, J. D. Kennedy, M. Thornton-Pett, and J. D. Woollins, *J. Chem. Soc., Dalton Trans.*, 1985, 2407.
54 J. E. Crook, N. N. Greenwood, J. D. Kennedy, and W. S. McDonald, *J. Chem. Soc., Chem. Commun.*, 1981, 933.
55 M. A. Beckett, N. N. Greenwood, J. D. Kennedy, P. A. Salter, and M. Thornton-Pett, *J. Chem. Soc., Chem. Commun.*, 1986, 556.
56 J. Bould, N. N. Greenwood, and J. D. Kennedy, *J. Chem. Soc., Dalton Trans.*, 1982, 481.
57 B. M. Graybill, J. K. Ruff, and M. F. Hawthorne, *J. Am. Chem. Soc.*, 1961, **83**, 2669.
58 A. R. Siedle, G. M. Bodner, A. R. Garber, and L. J. Todd, *Inorg. Chem.*, 1974, **13**, 1756.
59 S. Heřmánek, J. Fusek, B. Štíbr, J. Plešek, and T. Jelínek, *Polyhedron*, 1986, **5**, 1873.
60 G. M. Bodner, F. R. Scholer, L. J. Todd, L. E. Senor, and J. C. Carter, *Inorg. Chem.*, 1971, **10**, 942.
61 J. Rogozinski, M.Sc. Thesis, University of Leeds, 1984.
62 R. E. Williams, *Prog. Boron Chemistry*, 1964, **1**, 417.
63 J. D. Kennedy and J. Staves, *Z. Naturforsch., Teil B*, 1979, **34**, 808.
64 J. D. Kennedy and N. N. Greenwood, *Inorg. Chim. Acta*, 1980, **38**, 93.
65 J. D. Kennedy and B. Wrackmeyer, *J. Magn. Reson.*, 1980, **38**, 529.
66 A. Modinos and P. Woodward, *J. Chem. Soc., Dalton Trans.*, 1974, 2065.
67 N. Walker and D. Stuart, *Acta Crystallogr., Sect. A*, 1983, **39**, 158.
68 G. M. Sheldrick, SHELX 76, Program System for *X*-Ray Structure Determination, University of Cambridge, 1976.

Received 11*th August* 1987; *Paper* 7/1487